



Chinese Pharmaceutical Association
Institute of Materia Medica, Chinese Academy of Medical Sciences

Acta Pharmaceutica Sinica B

www.elsevier.com/locate/apsb
www.sciencedirect.com



ORIGINAL ARTICLE

Overexpressed SIRT6 ameliorates doxorubicin-induced cardiotoxicity and potentiates the therapeutic efficacy through metabolic remodeling



Kezheng Peng^a, Chenye Zeng^a, Yuqi Gao^a, Binliang Liu^b, Liyuan Li^a, Kang Xu^a, Yuemiao Yin^a, Ying Qiu^c, Mingkui Zhang^d, Fei Ma^b, Zhao Wang^{a,*}

^aThe Ministry of Education Key Laboratory of Protein Science, School of Pharmaceutical Sciences, Tsinghua University, Beijing 100084, China

^bDepartment of Medical Oncology, National Cancer Center/National Clinical Research Center for Cancer/Cancer Hospital, Chinese Academy of Medical Sciences and Peking Union Medical College, Beijing 100021, China

^cSchool of Medicine, Tsinghua University, Beijing 100084, China

^dDepartment of Cardiac Surgery, First Hospital of Tsinghua University, Beijing 100016, China

Received 31 October 2022; received in revised form 12 February 2023; accepted 2 March 2023

KEY WORDS

SIRT6;
Doxorubicin;
Cardiotoxicity;
Antitumor efficacy;
Ellagic acid;
Mitochondrial homeostasis;
Glycolysis;
SGK1

Abstract Since the utilization of anthracyclines in cancer therapy, severe cardiotoxicity has become a major obstacle. The major challenge in treating cancer patients with anthracyclines is minimizing cardiotoxicity without compromising antitumor efficacy. Herein, histone deacetylase SIRT6 expression was reduced in plasma of patients treated with anthracyclines-based chemotherapy regimens. Furthermore, overexpression of SIRT6 alleviated doxorubicin-induced cytotoxicity in cardiomyocytes, and potentiated cytotoxicity of doxorubicin in multiple cancer cell lines. Moreover, SIRT6 overexpression ameliorated doxorubicin-induced cardiotoxicity and potentiated antitumor efficacy of doxorubicin in mice, suggesting that SIRT6 overexpression could be an adjunctive therapeutic strategy during doxorubicin treatment. Mechanistically, doxorubicin-impaired mitochondria led to decreased mitochondrial respiration and ATP production. And SIRT6 enhanced mitochondrial biogenesis and mitophagy by deacetylating and inhibiting *Sgk1*. Thus, SIRT6 overexpression coordinated metabolic remodeling from glycolysis to mitochondrial respiration during doxorubicin treatment, which was more conducive to cardiomyocyte metabolism, thus protecting cardiomyocytes but not cancer cells against doxorubicin-induced energy

*Corresponding author.

E-mail address: zwang@tsinghua.edu.cn (Zhao Wang).

Peer review under the responsibility of Chinese Pharmaceutical Association and Institute of Materia Medica, Chinese Academy of Medical Sciences.

<https://doi.org/10.1016/j.apsb.2023.03.019>

2211-3835 © 2023 Chinese Pharmaceutical Association and Institute of Materia Medica, Chinese Academy of Medical Sciences. Production and hosting by Elsevier B.V. This is an open access article under the CC BY-NC-ND license (<http://creativecommons.org/licenses/by-nc-nd/4.0/>).

deficiency. In addition, ellagic acid, a natural compound that activates SIRT6, alleviated doxorubicin-induced cardiotoxicity and enhanced doxorubicin-mediated tumor regression in tumor-bearing mice. These findings provide a preclinical rationale for preventing cardiotoxicity by activating SIRT6 in cancer patients undergoing chemotherapy, but also advancing the understanding of the crucial role of SIRT6 in mitochondrial homeostasis.

© 2023 Chinese Pharmaceutical Association and Institute of Materia Medica, Chinese Academy of Medical Sciences. Production and hosting by Elsevier B.V. This is an open access article under the CC BY-NC-ND license (<http://creativecommons.org/licenses/by-nc-nd/4.0/>).

1. Introduction

Doxorubicin (also known as adriamycin, Dox) and other anthracyclines are widely used as monotherapies or in combination with additional agents or antibodies to treat various solid and hematologic malignancies¹. However, Dox treatment is accompanied by multiple side effects, and the most severe side effect is chemotherapy-induced cardiotoxicity (CIC), which is an irreversible complication due to the use of some anticancer agents, including anthracyclines and trastuzumab². It has been well established that CIC is cumulative-dose dependent and can be either in both acute and chronic forms, including aberrant arrhythmias, ventricular dysfunction, and heart failure^{2,3}. Acute cardiotoxicity has been described as transient arrhythmias and left ventricular dysfunction that occurs within days of treatment⁴. Chronic cardiotoxicity is more common than acute cardiotoxicity and can occur years after exposure to anthracyclines (median of 7 years after treatment)⁵. In cancer patients over 65 years of age and treated with commonly used doses of anthracyclines, the incidence of anthracycline-related heart failure can be as high as 10%⁶. Indeed, cardiovascular disease is the leading cause of mortality in older cancer survivors, contributing more than cancer mortality⁷. Despite the potent efficacy of anthracyclines as cancer treatments, severe cardiotoxicity and a narrow therapeutic window remain problematic and require specific management⁸.

Nowadays, clinical cardio-oncology programs have been established to understand the mechanism of CIC⁸. Although angiotensin-converting enzyme inhibitors and angiotensin receptor blockers were recommended to treat CIC, the therapeutic effects remain limited⁷. Therefore, other interventions that antagonize cardiotoxicity have intrigued both basic and clinical researchers for many years. For example, many chemotherapeutics, including Dox, can activate the transcription factor p53 in both cancer cells and cardiomyocytes, which subsequently leads to tumor regression and cardiotoxicity, respectively^{9,10}. Since p53 plays a crucial role in cardiac function¹¹, some investigators have attempted to antagonize Dox-induced cardiotoxicity by inhibiting p53 activation¹⁰. However, this approach does not seem to be suitable for preventing cardiotoxicity in cancer patients as p53 inhibition also promotes tumor growth^{9,12}. Most notably, a study reported that p53 inhibition exhibited cardioprotection during Dox treatment and, paradoxically, enhanced cardiotoxicity long after the cessation of treatment¹³. Therefore, designing appropriate therapies against Dox-induced cardiotoxicity without compromising antitumor efficacy is a major challenge¹⁴.

As a non-pharmacological intervention, caloric restriction (CR) has been confirmed to effectively delay aging and treat diseases such as diabetes, cancers, heart disease, neurodegeneration and hypertension¹⁵. Some preclinical evidence suggests that short-term starvation not only protects normal cells

against high-dose chemotherapy but also sensitizes a range of cancer cell types to chemotherapy^{16–18}. A recent study showed that short-term fasting protected mice against the toxicity associated with chemotherapy and enhanced therapeutic efficacy¹⁹. Notably, a prospective clinical trial in patients with breast cancer confirmed that a diet that mimicked fasting potentiated the therapeutic efficacy of chemotherapy, including Dox, and curtailed chemotherapy-induced toxicity in T lymphocytes¹⁹. Thus, both preclinical and clinical studies have confirmed that CR not only exerts effective anticarcinogenic effects but also significantly ameliorates chemotherapy-induced toxicity. However, the clinical application of CR remains limited since the long-term sustainability of CR may be difficult for most patients²⁰.

Current evidence suggests that the histone deacetylase SIRT6 can mimic the effects of CR on lifespan extension and improve glucose homeostasis^{21,22}. As a major target of CR, SIRT6 catalyzes the deacetylation of lysines 9, 18, and 56 of histone H3 (H3K9ac, H3K18ac and H3K56ac), thus regulating numerous biological processes, such as DNA repair, glucose/lipid metabolism and inflammation^{23–27}. Our previous study confirmed that SIRT6 attenuated cisplatin-induced kidney injury by deacetylating and inhibiting the expression of ERK1/2²⁸. Moreover, SIRT6 has been reported to be a tumor suppressor gene in many cancers, and cancer patients who express higher levels of SIRT6 have significantly lower relapse rates^{29,30}. Thus, we hypothesized that SIRT6 overexpression could alleviate cardiac dysfunction induced by Dox, while enhancing the antitumor efficacy of Dox, which may be similar to the phenotype induced by CR^{16–19}. To investigate this hypothesis, further experiments were conducted to confirm the implications of concurrent Dox administration and SIRT6 activation, and to critically evaluate and ensure that the antitumor efficacy of Dox remained uncompromised. Furthermore, the molecular mechanism underlying the differential SIRT6-mediated response to Dox in cardiomyocytes and cancer cells was explored.

2. Materials and methods

2.1. Clinical samples

This study was approved by the Institutional Review Boards of Cancer Hospital, Chinese Academy of Medical Sciences (No. NCC201712029), and the protocol has been registered on ClinicalTrials.gov with the number NCT03537339. Written informed consent was obtained from all patients, and this study conformed to the guidelines outlined in the Declaration of Helsinki. Ten breast cancer patients received 8 cycles of postoperative adjuvant AC-T chemotherapy (epirubicin 90 mg/m² and cyclophosphamide 600 mg/m² on Day 1, repeated every 14 (dose-density) or 21 days for 4 cycles, followed by paclitaxel 175 mg/m²

on Day 1 and repeated every 14 days for 4 cycles). Venous blood samples were collected prior to chemotherapy administration and after the first 4 cycles of anthracyclines-based chemotherapy regimens. SIRT6 expression was measured by ELISA kit (ThermoFisher, USA) according to the manufacturer's instructions. Lactate concentration was measured by L-lactate Assay Kit (BioAssay Systems, USA) as described in supplementary material.

2.2. Animal study

All animal experiments were performed according to the animal welfare and handling guidelines and were approved by the Institutional Animal Care and Use Committees of Tsinghua University. All mice were housed in an environmentally controlled animal facility (SPF) at Tsinghua University, which was maintained at a room temperature of 22–23 °C, with a 12 h light/dark cycle, and a normal diet and purified water ad libitum. The laboratory animal facility at Tsinghua University was accredited by the Institutional Animal Care and Use Committee (IACUC) and the Association for Assessment and Accreditation of Laboratory Animal Care International (AAALAC). All mice were randomly divided into groups and acclimatized to the laboratory environments for at least 7 days before the experiments.

2.3. Generation of transgenic mice

SIRT6 transgenic mice and SIRT6-knockout mice were generated in the C57BL/6 mouse strain as previously described²⁸. Briefly, cDNA was amplified from a plasmid encoding mouse SIRT6 and was subcloned into the cytomegalovirus promoter vector, and SIRT6 transgenic mice were generated according to the standard protocol of Cyagen Transgenic Animal Center (China). Moreover, SIRT6^{tm1.1Cxd} mice were obtained from Jackson Laboratory (USA) and mated with cytomegalovirus-cyclization recombination enzyme mice to obtain homozygotes. SIRT6^{+/-} male mice were mated with SIRT6^{+/-} female mice to obtain knockout (SIRT6^{-/-}) and wild-type (SIRT6^{+/+}) mice. The indicated mice were used for the isolation of primary cardiomyocytes and generation of a cardiotoxicity model, and total protein was isolated from the tails to confirm the levels of SIRT6 overexpression or knockout by Western blotting.

2.4. In vivo cardiotoxicity model

SIRT6 transgenic mice and wild-type littermates (6 weeks old, 20–25 g) were used to establish chronic (5-week low-dose treatment protocol) and acute (2-week high-dose treatment protocol) cardiotoxicity models. For the chronic cardiotoxicity model, Dox (4 mg/kg/week, Selleck, USA) dissolved in saline was administered by intravenous injection for 5 weeks, and the total cumulative dose was 20 mg/kg^{12,31}. After the mice were treated for 5 weeks, cardiac function was examined by echocardiography. Blood samples were collected from the orbit to measure biochemical parameters using an automatic biochemical analyzer. After the mice were euthanized by sodium pentobarbital (200 mg/kg, intraperitoneal injection), the hearts were excised and stored at -80 °C or fixed in 4% paraformaldehyde buffer for further experiments. For the acute cardiotoxicity model, Dox (20 mg/kg/week, Selleck) dissolved in saline was administered by intravenous injection for 2 weeks, and survival was observed daily¹⁷.

2.5. Tumor inoculation and treatment

Wild-type C57BL/6 mice (male, 6 weeks old, 25 g) were purchased from the Experimental Animal Center of Tsinghua University. LLC-Luc cells (LLC cells stably expressing the luciferase gene) were harvested and resuspended in phosphate-buffered saline and Matrigel (Corning, USA) at a 1:1 ratio, and 200 µL of the resuspended cells (containing 1.5×10^6 cells) was inoculated subcutaneously into the forelimb of each mouse. After tumors became visible (approximately 7 days), the mice were randomly divided into different groups and treated with Dox and/or ellagic acid for 14 days. Dox (10 mg/kg/week, Selleck) dissolved in saline was administered by intravenous injection, and the total cumulative dose was 20 mg/kg^{12,31}. Ellagic acid (100 mg/kg/2 days, MedChemExpress, USA) was dissolved in 0.5% carboxymethylcellulose (Selleck) and 0.1% Tween 80 (MedChemExpress), and administered by oral gavage. The mice in the control group were administered the solvent as a placebo. Tumor growth was monitored at different time points by bioluminescence imaging using the IVIS Lumina Imaging System (PerkinElmer, USA), and D-Luciferin potassium (PerkinElmer) was administered by intraperitoneal injection at a concentration of 160 mg/kg. At treatment termination, cardiac function was examined by echocardiography. After the mice were euthanized by sodium pentobarbital (200 mg/kg, intraperitoneal injection), the hearts and tumors were excised and stored at -80 °C or fixed in 4% paraformaldehyde buffer for further experiments.

2.6. Cell culture

Murine HL-1 cardiomyocytes, murine Lewis lung carcinoma (LLC) cells, 4T1 murine breast cancer cells, and B16-F10 murine melanoma cells were obtained from the Cell Bank of Type Culture Collection of the Chinese Academy of Sciences. All cell lines were cultured in Dulbecco's modified Eagle's medium (DMEM, Gibco, USA) containing 10% fetal bovine serum (FBS, Corning) and 1% penicillin–streptomycin (PS, Gibco) in a CO₂ incubator with saturated humidity, 5% CO₂ and 37 °C, except 4T1 cells, which were cultured in RPMI-1640 medium (Gibco). No cell line was continuously passaged more than 15 times.

Primary murine cardiomyocytes were isolated from neonatal mice by a standard procedure with minimal modifications³². In brief, hearts were excised from 1- to 3-day-old C57BL/6 mice, washed twice with PBS and digested with 0.06% trypsin (Gibco) containing 0.1% type II collagenase (Solarbio, China). Digestion was continued for 8 min in a 37 °C water bath, and after digestion, the tissues were further digested a total of 6 more times. After being centrifuged, the cardiomyocytes were cultured in DMEM containing 10% FBS and 1% PS, and the cells formed a monolayer with synchronized beating.

Other detailed methods are provided in the [Supporting Information](#).

2.7. Measurements of OCR, ECAR and ATP production rates

The oxygen consumption rate (OCR), extracellular acidification rate (ECAR), and real-time ATP production rate were measured by a Seahorse XF96 extracellular-flux analyzer (Agilent Technologies, USA) according to the manufacturer's instructions³³. In brief, primary cardiomyocytes or LLC cells were seeded into XF96 Cell Culture Microplates (Agilent Technologies) at a density of 5000 or 7000 cells/well and cultured at 37 °C for 24 h.

After the cells were treated with or without 0.5 $\mu\text{mol/L}$ Dox for 12 h, the culture medium was changed to specialized medium as described before the cells were analyzed by a Seahorse extracellular flux analyzer. L-Glutamine (4 mmol/L, Sigma, USA) was added to Seahorse XF Base Medium (Agilent Technologies) to obtain the Glycolysis Stress Test Assay Medium. Glucose (25 mmol/L, Sigma), sodium pyruvate (1 mmol/L, Sigma) and L-glutamine (4 mmol/L, Sigma) were added to Seahorse XF Base Medium (Agilent Technologies) to obtain the Mitochondrial Stress Test Assay Medium. Seahorse XF DMEM (Agilent Technologies) containing 10 mmol/L glucose, 1 mmol/L sodium pyruvate and 2 mmol/L L-glutamine was used in the real-time ATP production rate assay. The pH of all assay media was checked and adjusted to 7.40 ± 0.05 . The ECAR was determined by treating cells with glucose (10 mmol/L, Sigma), oligomycin (2 $\mu\text{mol/L}$, Sigma) and 2-deoxyglucose (2-DG, 100 mmol/L, Sigma). The OCR was determined by treating the cells with oligomycin (2 $\mu\text{mol/L}$, Sigma), carbonyl cyanide 4-(trifluoromethoxy)phenylhydrazone (FCCP, 1.5 $\mu\text{mol/L}$, Sigma), rotenone (1 $\mu\text{mol/L}$, Sigma) and antimycin A (1 $\mu\text{mol/L}$, Sigma). The real-time ATP production rate was measured by treating the cells with oligomycin (2 $\mu\text{mol/L}$, Sigma), rotenone (1 $\mu\text{mol/L}$, Sigma) and antimycin A (1 $\mu\text{mol/L}$, Sigma). All results were normalized by a BCA protein assay kit (Solarbio) according to the manufacturer's protocol and analyzed by Wave software (Agilent Technologies).

2.8. Statistical analysis

All data were statistically analyzed using GraphPad Prism software. Experimental results containing more than two groups were analyzed by one-way analysis of variance (ANOVA), and multiple comparisons between the groups were conducted by the Bonferroni method. Two-tailed *t* test were performed for two-group analysis. All experiments were conducted in triplicate, or at least three parallel experiments were performed. The results are expressed as the mean \pm standard deviation (SD) or standard error of the mean (SEM), and a value of $P < 0.05$ was considered statistically significant.

3. Results

3.1. Decreased SIRT6 expression were observed in plasma of anthracyclines-treated cancer patients

SIRT6 has recently been measured in the blood to evaluate health or disease state^{34–36}. For example, decreased serum SIRT6 expression is observed in patients with stable angina as well as patients with acute coronary³⁷. To confirm the clinical relevance of SIRT6 in Dox-induced cardiotoxicity, we examined the expression levels of SIRT6 and the concentration of lactate in the plasma of breast cancer patients. The characteristics of patients were shown in Supporting Information Table S1. After 4 cycles of anthracyclines-based chemotherapy regimens, decreased levels of SIRT6 were observed in plasma from patients, compared with the plasma obtained from those patients before treatment (Fig. 1A), suggesting that SIRT6 expression was inhibited by chemotherapy treatment. Moreover, the lactate concentration was significantly higher in the plasma from patients after treatment than before treatment (Fig. 1B), which confirmed that the increase in glycolysis was associated with chemotherapy treatment. These results indicate that the reduction in SIRT6 and increase in glycolysis are associated with anthracyclines-induced toxicity in humans.

3.2. SIRT6 overexpression ameliorates Dox-induced cytotoxicity in cardiomyocytes and exacerbates Dox-induced cytotoxicity in cancer cells

To examine whether SIRT6 overexpression could ameliorate Dox-induced cardiotoxicity, we isolated primary cardiomyocytes from SIRT6 transgenic (TG) mice and wild-type (WT) littermates and treated the cells with different concentrations of Dox. The viability rates of TG cardiomyocytes were significantly higher than those of WT cardiomyocytes after Dox treatment (Fig. 2A). Similar results were observed in cardiac fibroblasts, the cardiac fibroblasts isolated from SIRT6 TG mice were less sensitive to Dox than the cardiac fibroblasts isolated from WT littermates (Fig. 2A). We next generated HL-1 murine cardiomyocytes with lentivirus-mediated ectopic SIRT6 overexpression and found that

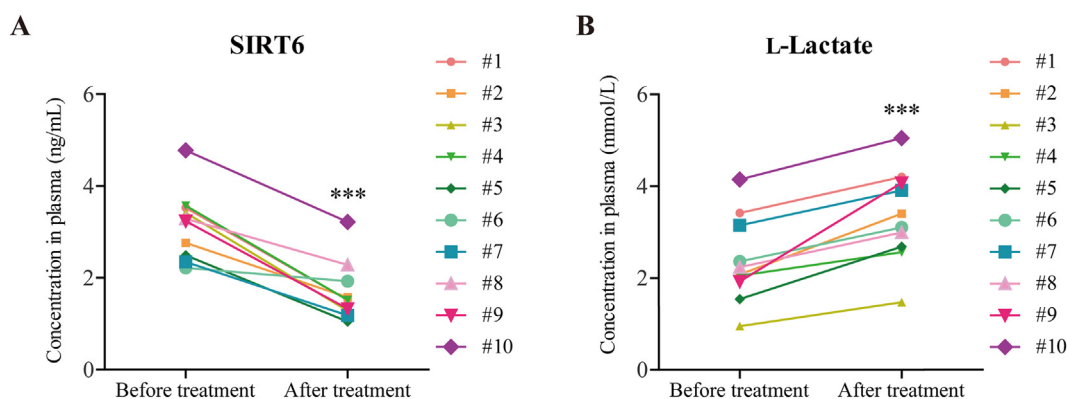


Figure 1 Decreased SIRT6 expression and increased lactate accumulation were observed in the plasma of anthracyclines-treated cancer patients. (A) Ten breast cancer patients received postoperative adjuvant therapy with anthracyclines-based chemotherapy regimens, and plasma was collected before and after chemotherapy from same patients. SIRT6 expression in the plasma of cancer patients was measured by ELISA ($n = 10$ patients). (B) Lactate concentration in the plasma of cancer patients was measured ($n = 10$ patients). The data are expressed as the mean \pm standard deviation. Two-tailed paired *t* tests were performed to determine significant differences. $***P < 0.001$.

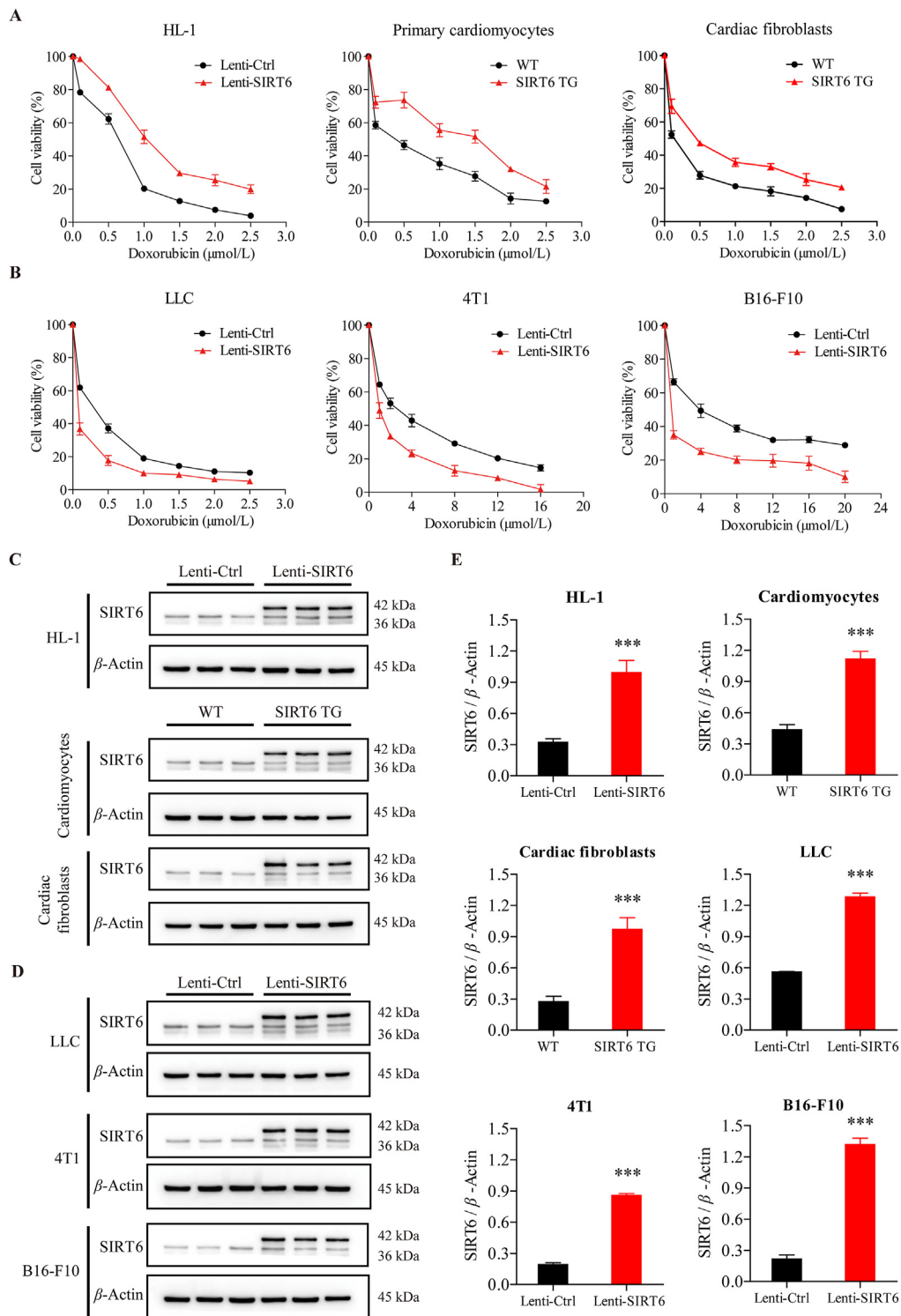


Figure 2 Ectopic SIRT6 overexpression ameliorates Dox-induced cytotoxicity in cardiomyocytes but exacerbates Dox-induced cytotoxicity in cancer cells. (A, B) After treatment with different concentrations of doxorubicin (Dox) for 24 h, the viability of primary cardiomyocytes and cardiac fibroblasts isolated from SIRT6 transgenic (TG) mice and wild-type (WT) littermates, mouse cardiomyocyte HL-1 cells, mouse Lewis lung carcinoma LLC cells, mouse breast cancer 4T1 cells, and mouse melanoma B16-F10 cells infected with lentivirus containing SIRT6 vector (Lenti-SIRT6) or control vector (Lenti-Ctrl) was assessed by the CCK-8 method ($n = 3$ different experiments). (C, D) The protein expression of SIRT6 in HL-1 cells, primary cardiomyocytes, cardiac fibroblasts, LLC cells, 4T1 cells, and B16-F10 cells was detected by Western blotting. β -Actin was used as a loading control. (E) Semiquantitative analyses of bands were performed using ImageJ software ($n = 3$ different experiments). The data are expressed as the mean \pm standard deviation. Two-tailed unpaired t tests were performed to determine significant differences. *** $P < 0.001$ compared to the control group.

HL-1 cells with SIRT6 overexpression were less susceptible to Dox than control HL-1 cells (Fig. 2A). The levels of SIRT6 overexpression were analyzed by Western blotting (Fig. 2C and E). These findings confirmed that SIRT6 overexpression could ameliorate Dox-induced cardiotoxicity *in vitro*.

To explore whether SIRT6 overexpression could affect the anticancer efficacy of Dox, we generated murine Lewis lung carcinoma (LLC) cells, 4T1 murine breast cancer cells, and B16-F10 murine melanoma cells with lentivirus-mediated ectopic SIRT6 overexpression. Conversely, cancer cells overexpressing SIRT6 were more sensitive to Dox than control cells (Fig. 2B), suggesting that SIRT6 overexpression can exacerbate Dox-induced cytotoxicity in cancer cells. The levels of SIRT6 overexpression were analyzed by Western blotting (Fig. 2D and E). Thus, the results in Fig. 2 demonstrate that SIRT6 overexpression could ameliorate Dox-induced cytotoxicity in cardiomyocytes and potentiate the anticancer efficacy of Dox in cancer cells.

3.3. SIRT6 overexpression ameliorates Dox-induced cardiotoxicity in mice

To explore whether SIRT6 overexpression could ameliorate Dox-induced cardiotoxicity *in vivo*, we generated SIRT6 transgenic mice and established chronic (5-week low-dose treatment protocol) and acute (2-week high-dose treatment protocol) Dox-induced cardiotoxicity mouse models^{12,17,31}.

In the chronic cardiotoxicity model (Fig. 3A), TG mice and WT littermates were treated with low doses of Dox (4 mg/kg/week) or saline for 5 weeks, and the total cumulative dose was 20 mg/kg. After treatment, cardiac function was measured using echocardiography as assessed by ejection fraction (EF), fractional shortening (FS), diastolic left ventricular anterior wall thickness (LVAWd) and diastolic left ventricular internal diameter (LVIDd). After 5 weeks of treatment, WT mice treated with Dox showed significant decreases in EF, FS, LVAWd and LVIDd compared to those of saline-treated WT mice (Fig. 3C and D), demonstrating that Dox could induce cardiac dysfunction in WT mice. In contrast, defects in cardiac function were not evident in Dox-treated TG mice compared to saline-treated TG mice (Fig. 3C and D). Notably, cardiac dysfunction in Dox-treated WT mice was more severe than that in Dox-treated TG mice, suggesting that SIRT6 overexpression could ameliorate Dox-induced cardiac dysfunction. Moreover, biochemical parameters associated with heart failure, including LDH, LDH1, CK and CK-MB, were used to assess the cardiotoxicity of Dox. Consistent with the echocardiography results, Dox treatment significantly increased the concentrations of LDH, LDH1, CK and CK-MB in WT mice (Fig. 3B and Supporting Information Fig. S1A). The concentrations of LDH, LDH1, CK and CK-MB in Dox-treated TG mice were significantly lower than those in Dox-treated WT mice, which further confirmed the cardioprotective effect of SIRT6 (Fig. 3B and Fig. S1A). In addition, Dox treatment increased apoptosis and fibrosis in the myocardium of WT mice, as assessed by TUNEL and Masson trichrome staining, respectively (Fig. 3E and F). In contrast to Dox-treated WT mice, Dox-treated TG mice were relatively resistant to Dox-induced apoptosis and fibrosis (Fig. 3E and F), suggesting that SIRT6 overexpression could decrease Dox-induced cardiomyocyte apoptosis and cardiac fibrosis. The changes in body weight were recorded weekly (Fig. S1B). SIRT6 has been shown to inhibit phosphorylation and nuclear localization of Smad signaling, which alleviated liver fibrosis³⁸. We reconfirmed this result in cardiac fibroblasts, and found that

SIRT6 overexpression increased the phosphorylation levels of Smad 2 and Smad 3 (Supporting Information Fig. S2), which may be the mechanisms underlying the improved cardiac fibrosis in the Dox-treated SIRT6 TG mice.

In the acute cardiotoxicity model (Fig. 3A), after treatment with high doses of Dox (20 mg/kg/week) or saline for 2 weeks, the survival of TG mice and WT littermates was observed daily. No animals died after treatment with saline (data not shown). Among the Dox-treated animals, TG mice survived much longer than WT littermates (Fig. 3G). This protective effect against high-dose Dox was observed in both sexes (Fig. 3G). The changes in body weight were recorded weekly (Fig. S1C). These findings are consistent with our *in vitro* data and suggest that SIRT6 could be an effective therapeutic target for the treatment of Dox-induced cardiotoxicity.

3.4. SIRT6 overexpression potentiates antitumor efficacy of Dox in mice

To explore whether SIRT6 overexpression could potentiate anti-tumor efficacy of Dox *in vivo*, wild-type C57BL/6 mice were injected with LLC cells with SIRT6 overexpression or control LLC cells. The tumor-bearing mice were treated with Dox (10 mg/kg/week) or saline for 2 weeks, and the total cumulative dose was 20 mg/kg (Fig. 4A). Luminescence analysis of tumors showed that treatment with Dox suppressed tumor growth compared to saline treatment (Fig. 4B and C). Notably, SIRT6 overexpression significantly potentiated Dox-mediated tumor regression (Fig. 4B and C). Moreover, the results of tumor weight showed that SIRT6 overexpression did not independently decrease tumor weight compared to saline treatment, but effectively enhanced the anti-tumor effect of Dox (Fig. 4D and E). These results above suggested that Dox exhibited greater antitumor efficacy in LLC tumors with SIRT6 overexpression than in control LLC tumors.

In addition, Dox treatment inhibited proliferative activity and increased apoptosis in control LLC tumors, as measured by Ki67 immunofluorescence staining and TUNEL staining, respectively (Fig. 4F and G). Notably, SIRT6 overexpression did not independently inhibit proliferative activity, but significantly potentiated Dox-mediated anti-proliferative and pro-apoptotic activity in the tumors (Fig. 4F and G), suggesting that SIRT6 overexpression could significantly potentiate the antitumor efficacy of Dox. These results confirm that SIRT6 overexpression could be an adjunctive therapeutic strategy during treatment of Dox.

3.5. Dox impairs mitochondrial respiration and mtDNA integrity to induce cytotoxicity in cardiomyocytes and cancer cells

To explore the molecular mechanism underlying Dox-induced cardiotoxicity, we performed RNA sequencing on primary cardiomyocytes isolated from WT mice. Dox treatment induced a large number of differentially expressed genes in cardiomyocytes compared to untreated cardiomyocytes (Fig. 5A). Kyoto Encyclopedia of Genes and Genomes (KEGG) pathway analysis indicated that these genes were highly enriched in metabolic pathways (Fig. 5B), including the regulation of carbohydrate metabolism, lipid metabolism and amino acid metabolism, suggesting that Dox-induced metabolic changes may be responsible for its cardiotoxicity.

To confirm these Dox-induced metabolic changes, we examined mitochondrial respiration and glycolysis in cardiomyocytes and LLC cells with a Seahorse extracellular-flux analyzer. Dox-treated cardiomyocytes exhibited marked reductions in basal

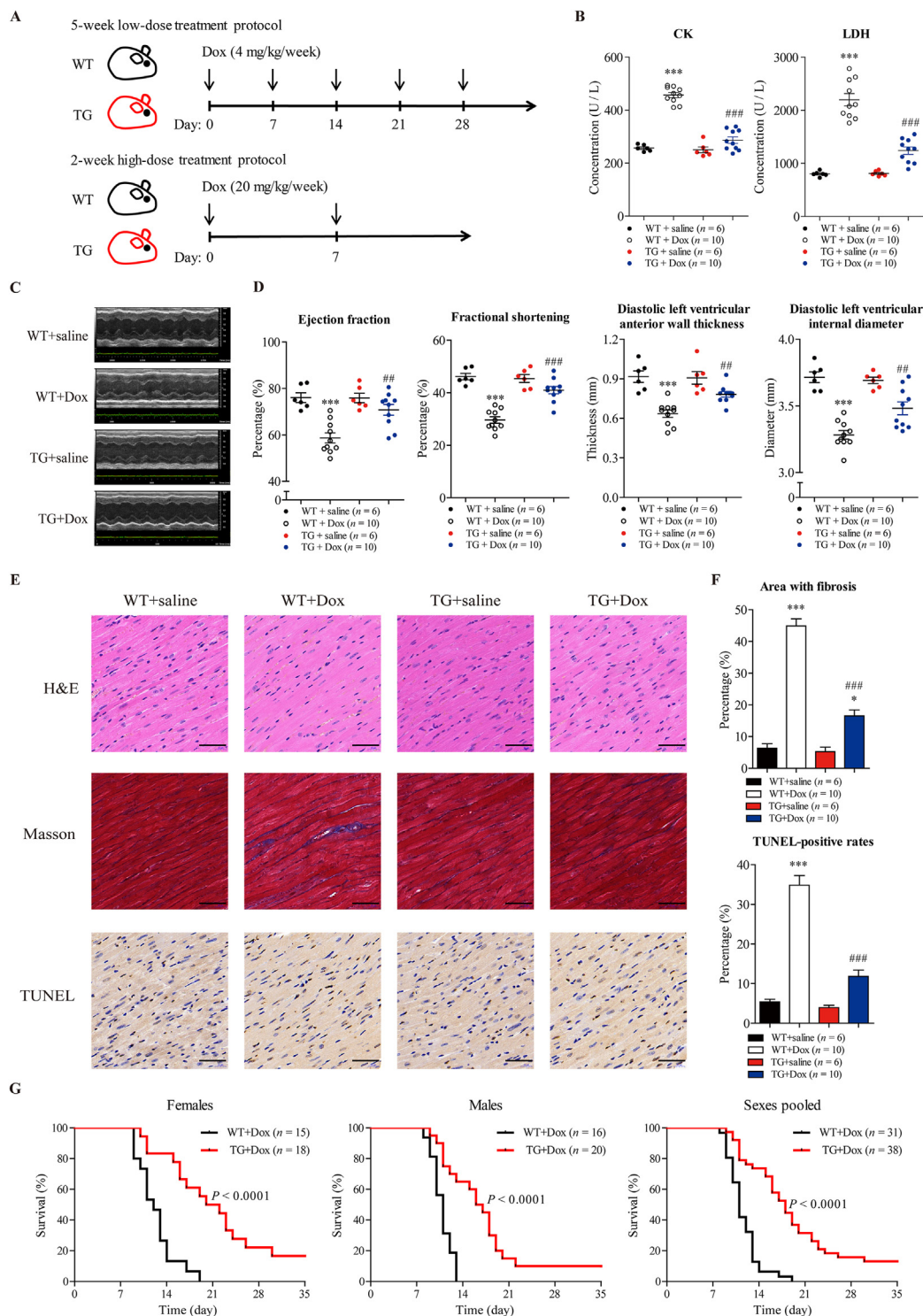


Figure 3 SIRT6 overexpression ameliorates Dox-induced cardiotoxicity in mice. (A) The chronic low-dose treatment protocol and acute high-dose treatment protocol are shown. In the chronic treatment protocol, SIRT6 transgenic mice and wild-type littermates were injected with Dox (4 mg/kg/week, i.v.) or saline for 5 weeks, and the total cumulative dose was 20 mg/kg. In the acute treatment protocol, wild-type and SIRT6 transgenic mice were injected with Dox (20 mg/kg/week, i.v.) or saline for 2 weeks. (B) In the chronic treatment protocol, biochemical parameters associated with heart failure were measured in the plasma of the mice. The levels of CK-MB and LDH1 are shown in Fig. S1 ($n = 6$ or 10 animals per group). (C, D) In the chronic treatment protocol, cardiac function was measured using echocardiography and was assessed by ejection fraction, fractional shortening, diastolic left ventricular anterior wall thickness, and diastolic left ventricular internal diameter ($n = 6$ or 10 animals per group). (E) In the chronic treatment protocol, fibrosis, apoptosis and cell morphology in cardiac tissue were measured by Masson trichrome staining, TUNEL and H&E staining, respectively. Representative images were shown. Scale bar = 50 μm . (F) Quantitative analyses of the fibrotic area (blue-stained) and TUNEL-positive cells (brown-stained) in E were performed by ImageJ software ($n = 6$ or 10 animals per group). The data

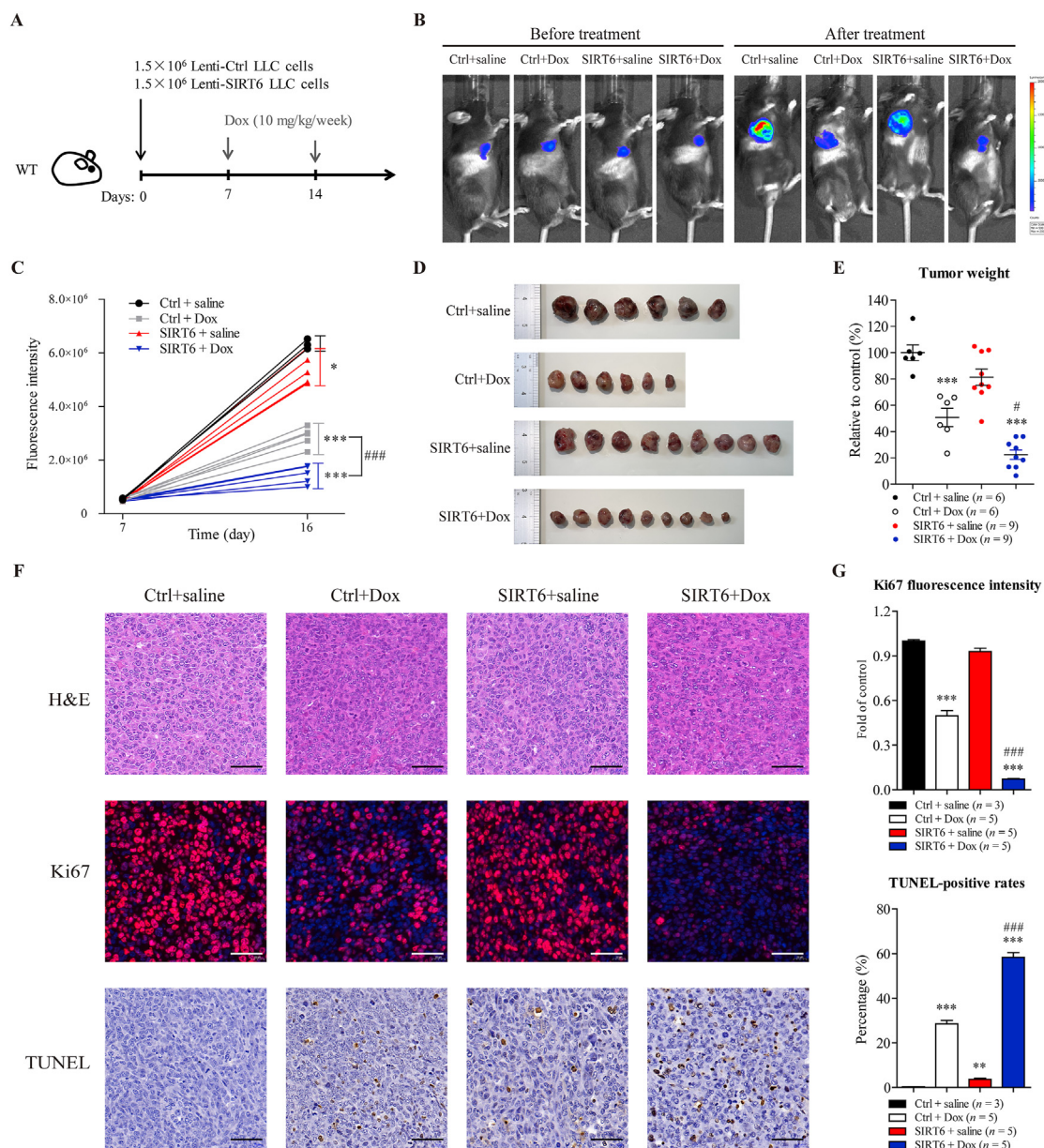


Figure 4 SIRT6 overexpression potentiates antitumor efficacy of Dox in mice. (A) The treatment protocol is shown. Wild-type C57BL/6 mice were inoculated subcutaneously with 1.5×10^6 LLC cells with lentivirus-mediated SIRT6 overexpression (Lenti-SIRT6) or control LLC cells (Lenti-Ctrl). After tumors became visible (approximately 7 days), the tumor-bearing mice were treated with Dox (10 mg/kg/week, i.v.) for 2 weeks, and the total cumulative dose was 20 mg/kg. (B, C) Tumor volume was visualized using the IVIS Imaging System before and after treatment, and representative bioluminescence images and quantitative analyses of the tumor-bearing mice are shown ($n = 3$ or 5 animals per group). (D, E) At treatment termination, tumors from each mouse were excised and weighed, and photographs of the tumors are shown ($n = 6$ or 9 animals per group). (F) Cell morphology, proliferative activity and apoptosis and in the tumors were measured by H&E, Ki67 immunofluorescence and TUNEL staining, respectively. Representative images are shown. Scale bar = 50 μ m. (G) Quantitative analyses of the fluorescence of Ki67 (red-stained) and TUNEL-positive cells (brown-stained) in F were performed by ImageJ software ($n = 3$ or 5 animals per group). The data are expressed as the mean \pm standard error of mean. One-way ANOVA followed by Bonferroni multiple comparisons were performed to determine significant differences. * $P < 0.05$, ** $P < 0.01$, and *** $P < 0.001$ compared to saline-treated control mice. # $P < 0.05$, ## $P < 0.01$, and ### $P < 0.001$ compared to Dox-treated control mice.

are expressed as the mean \pm standard error of mean. One-way ANOVA followed by Bonferroni multiple comparisons were performed to determine significant differences. * $P < 0.05$, ** $P < 0.01$, and *** $P < 0.001$ compared to saline-treated WT mice. # $P < 0.05$, ## $P < 0.01$, and ### $P < 0.001$ compared to Dox-treated WT mice. (G) In the acute treatment protocol, survival of wild-type and SIRT6 transgenic mice was observed daily ($n = 15$ to 20 animals per group). P values were calculated by the log-rank test.

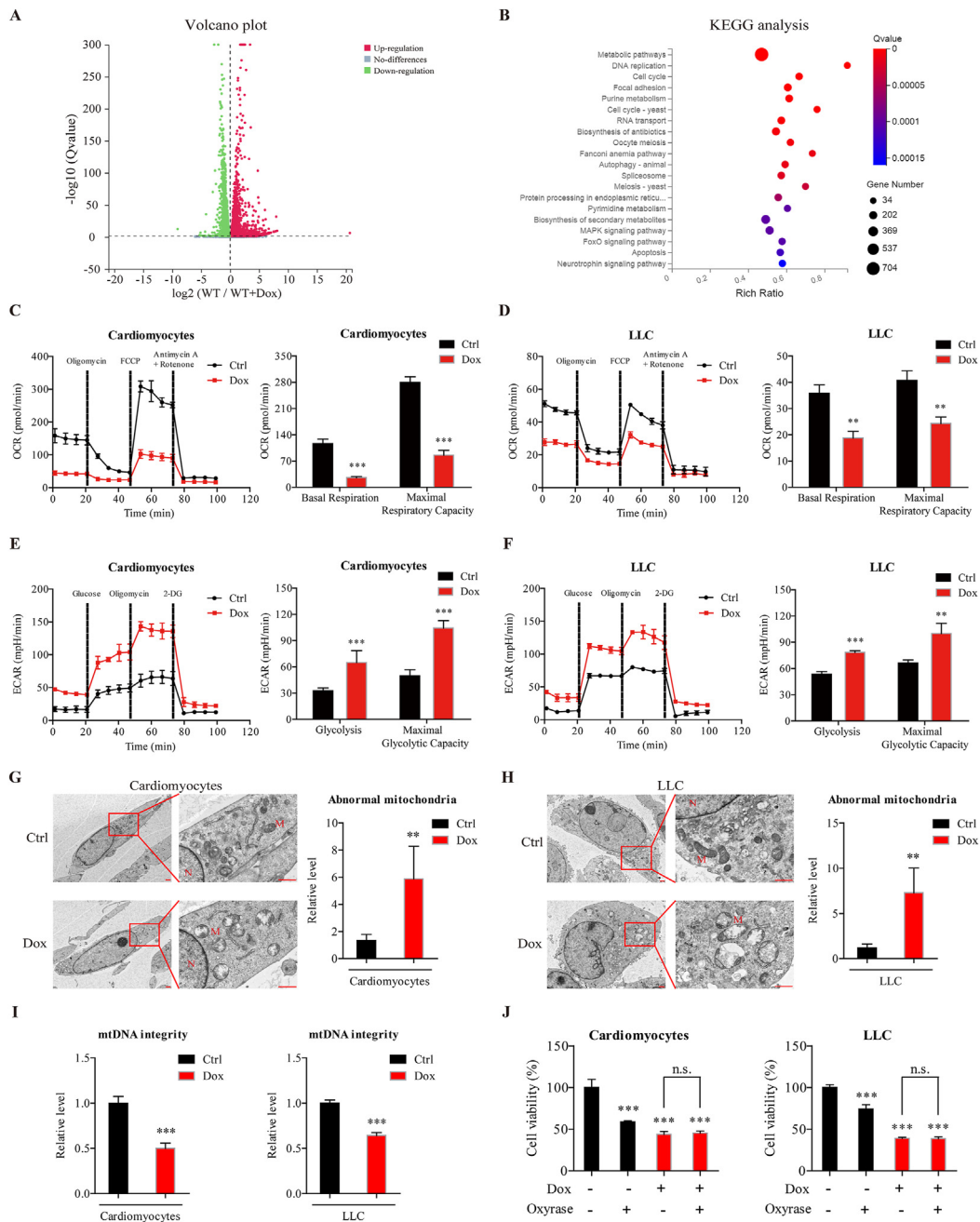


Figure 5 Dox impairs mitochondrial respiration and mtDNA integrity to induce cytotoxicity in cardiomyocytes and cancer cells. (A) RNA sequencing was performed on primary cardiomyocytes isolated from WT mice, after treated with Dox (0.5 $\mu\text{mol/L}$) or solvent for 24 h. Differentially expressed genes are shown in volcano plots. (B) Kyoto Encyclopedia of Genes and Genomes (KEGG) pathway analysis of differentially expressed genes. (C, D) The oxygen consumption rate (OCR) was measured by a Seahorse XF96 extracellular-flux analyzer after cardiomyocytes and LLC cells were treated with Dox (0.5 $\mu\text{mol/L}$) for 12 h ($n = 3$ different experiments). (E, F) The extracellular acidification rate (ECAR) was measured by a Seahorse XF96 extracellular-flux analyzer after cardiomyocytes and LLC cells were treated with Dox (0.5 $\mu\text{mol/L}$) for 12 h ($n = 3$ different experiments). (G, H) Representative electron microscopic images of cardiomyocytes and LLC cells after Dox treatment (0.5 $\mu\text{mol/L}$) for 24 h are shown. Scale bar = 1 μm . The number of abnormal mitochondria was quantified blindly in 5 images from different fields. (I) Mitochondrial DNA (mtDNA) integrity was determined after cardiomyocytes and LLC cells were treated with Dox (0.5 $\mu\text{mol/L}$) for 24 h ($n = 3$ different experiments). (J) Cell viability was measured by the CCK-8 assay after cardiomyocytes and LLC cells were treated with oxyrase and/or Dox (0.5 $\mu\text{mol/L}$) for 24 h ($n = 3$ different experiments). The data are expressed as the mean \pm standard deviation. Two-tailed unpaired t tests were performed to determine significant differences in C–I. One-way ANOVA followed by Bonferroni multiple comparisons were performed to determine significant differences in J. * $P < 0.05$, ** $P < 0.01$, *** $P < 0.001$ compared to the control group. n.s., no significance.

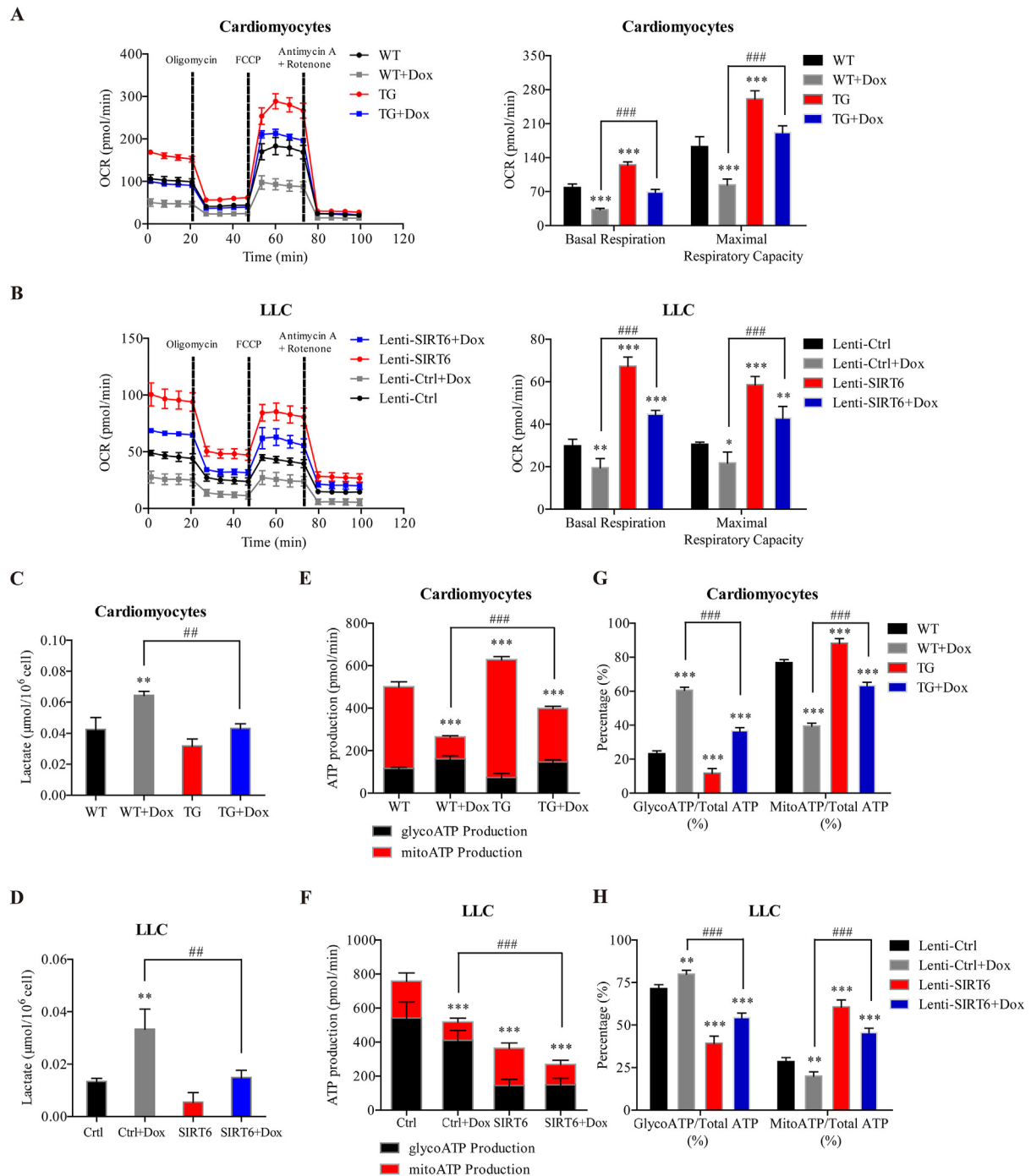


Figure 6 SIRT6 overexpression differentially regulates ATP production in cardiomyocytes and cancer cells during Dox treatment by enhancing mitochondrial respiration and inhibiting glycolysis. (A, B) Primary cardiomyocytes isolated from SIRT6 TG and WT littermates, LLC cells with lentivirus-mediated SIRT6 overexpression (Lenti-SIRT6) and control LLC cells (Lenti-Ctrl) were treated with Dox (0.5 $\mu\text{mol}/\text{L}$) for 12 h, and the oxygen consumption rate (OCR) was measured by a Seahorse XF96 extracellular-flux analyzer. (C, D) the lactate concentration was measured, (E–H) and the real-time ATP production rate assay was performed by a Seahorse XF96 extracellular-flux analyzer ($n = 3$ different experiments). The data are expressed as the mean \pm standard deviation. One-way ANOVA followed by Bonferroni multiple comparisons were performed to determine significant differences. * $P < 0.05$, ** $P < 0.01$, and *** $P < 0.001$ compared to the control group. # $P < 0.05$, ## $P < 0.01$, and ### $P < 0.001$ compared to the Dox-treated group.

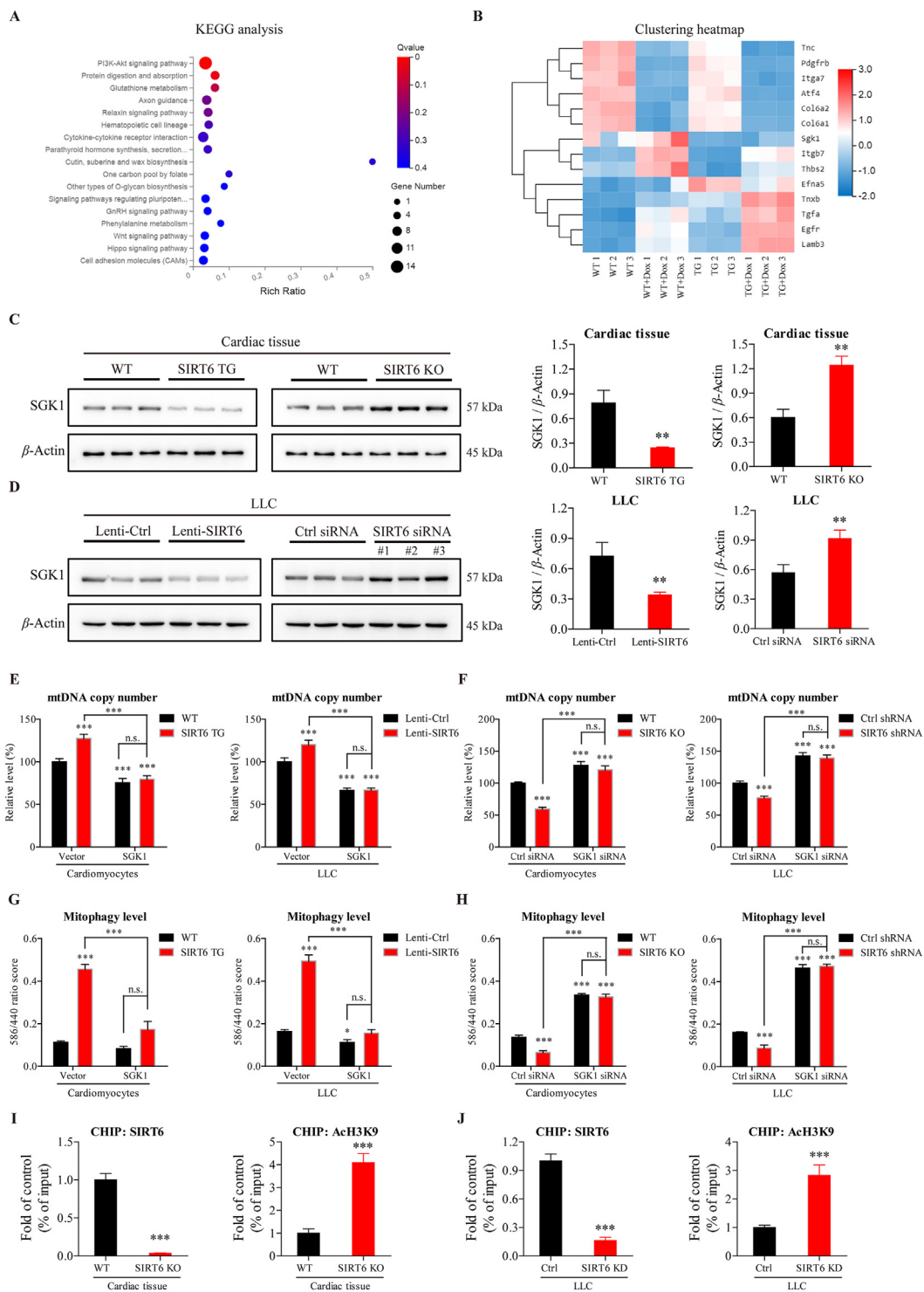


Figure 7 SIRT6 deacetylates and inhibits *Sgk1* to regulate mitochondrial biogenesis and mitophagy. (A) RNA sequencing was performed on primary cardiomyocytes isolated from SIRT6 TG and WT littermates. The differentially expressed genes were analyzed by Kyoto Encyclopedia of Genes and Genomes (KEGG) pathway analysis. (B) The heatmap that was created from the clustering of 14 enriched genes in the PI3K/Akt signaling pathway, which as the most highly enriched pathway identified by KEGG analysis. (C, D) Western blotting analysis of SGK1 in (C) the cardiac tissue of SIRT6 TG mice and WT littermates, as well as SIRT6-knockout (KO) mice and WT littermates, (D) LLC cells with lentivirus-mediated SIRT6 overexpression (Lenti-SIRT6) and control LLC cells (Lenti-Ctrl), and LLC cells transfected with SIRT6 siRNA or control siRNA. β -Actin was used as a loading control. Semiquantitative analyses of bands were performed using ImageJ software ($n = 3$ different experiments). (E, F) Mitochondrial mass as assessed by mitochondrial DNA (mtDNA) copy number was measured in (E) cells infected with lentivirus containing the SGK1 vector or control vector and (F) cells transfected with SGK1 siRNA or control siRNA ($n = 3$ different experiments). (G, H) After the cells were transfected with a mitophagy reporter (mKeima-Red-IRES-Park2), the mitophagy level was assessed by

respiration and maximal respiratory capacity compared to vehicle-treated cells, as assessed by a reduction in the oxygen consumption rate (Fig. 5C), which was consistent with previous reports¹⁴. Similar to the results in cardiomyocytes, Dox treatment significantly decreased basal respiration and maximal respiratory capacity in LLC cells compared to vehicle-treated cells (Fig. 5D). These results confirm that mitochondrial respiration was significantly reduced by Dox treatment in both cardiomyocytes and LLC cells. In addition, glycolysis and the maximal glycolytic capacity were significantly increased in both cardiomyocytes and LLC cells after Dox treatment, as assessed by the increased extracellular acidification rate (Fig. 5E and F), which suggested that the adopted increase in glycolysis compensate for the loss of energy production by mitochondrial respiration.

To elucidate the reason for the reduction in mitochondrial respiration, we examined the effects of Dox on mitochondrial morphology by transmission electron microscopy (TEM). Increased numbers of abnormal mitochondria were observed in both cardiomyocytes and LLC cells after Dox treatment (Fig. 5G and H), which were characterized by marked vacuolation and swollen and disrupted cristae. A previous study indicated that Dox could intercalate mitochondrial DNA (mtDNA) and destroy mtDNA integrity^{31,39}. In this study, Dox treatment significantly decreased mtDNA integrity in both cardiomyocytes and LLC cells, compared to vehicle-treated cells (Fig. 5I). These results demonstrate that Dox impaired mitochondrial structure and mtDNA integrity, thus subsequently leading to impaired mitochondrial respiration. Notably, we also found that oxryase-induced hypoxia inhibited the viability of cardiomyocytes and LLC cells, but the inhibitory effects were not further altered in response to hypoxia and Dox co-treatment compared to Dox treatment alone (Fig. 5J), which suggested that Dox-mediated mitochondrial dysfunction may be responsible for its cytotoxic effects on cardiomyocytes and LLC cells.

Taken together, these results indicate that Dox-induced mtDNA damage severely impaired mitochondrial respiration, thus subsequently leading to a glycolytic shift to compensate for decreased mitochondrial respiration. Impaired mitochondrial respiration may mediate the cytotoxic effects of Dox in both cardiomyocytes and LLC cells.

3.6. SIRT6 overexpression differentially regulates ATP production in cardiomyocytes and cancer cells during Dox treatment by enhancing mitochondrial respiration and inhibiting glycolysis

It has been reported that SIRT6-deficient embryonic stem cells and cancer cells exhibit increased glycolysis and reduced mitochondrial respiration^{29,40}, which were similar to the Dox-induced metabolic phenotype observed in this study. Thus, we hypothesized that SIRT6 overexpression could reverse the glycolytic shift induced by Dox in cardiomyocytes and LLC cells. To investigate this hypothesis, we isolated primary cardiomyocytes from SIRT6

TG mice and WT littermates, and incubated LLC cells with SIRT6 overexpression lentiviral vectors. Basal respiration and maximal respiratory capacity were significantly impaired after cardiomyocytes and LLC cells were treated with Dox (Fig. 6A and B). Cardiomyocytes and LLC cells overexpressing SIRT6 exhibited marked increases in basal respiration and maximal respiratory capacity compared to control cells (Fig. 6A and B). Interestingly, the Dox-mediated reductions in basal respiration and maximal respiratory capacity were significantly reversed in cardiomyocytes and LLC cells overexpressing SIRT6 (Fig. 6A and B). In addition, SIRT6 overexpression significantly suppressed Dox-induced lactate accumulation in both cardiomyocytes and LLC cells (Fig. 6C and D), suggesting the inhibitory effects of SIRT6 overexpression on glycolysis. These results indicated that SIRT6 overexpression coordinates a switch from glycolysis to mitochondrial respiration, which could suppress Dox-induced glycolysis and reverse the Dox-mediated reduction in mitochondrial respiration.

Most cancer cells depend on glycolysis for ATP production, even in the presence of adequate oxygen, which is also known as the Warburg effect⁴¹. In contrast, mitochondrial respiration is used as the major energy source of cardiomyocytes under normal physiological conditions, while glycolysis contributes little to the ATP requirements of the heart⁴². Thus, we hypothesized that SIRT6-mediated metabolic remodeling from glycolysis to mitochondrial respiration is more suitable for the viability of cardiomyocytes than that of cancer cells during Dox treatment. To test this hypothesis, we analyzed the metabolic phenotype of cells overexpressing SIRT6 in the presence or absence of Dox. As expected, glycolysis provided 71.5% of the total energy requirement in untreated LLC cells but accounted for merely 23.2% of the total ATP production in untreated cardiomyocytes (Fig. 6E and F). Dox treatment decreased total ATP production in both cardiomyocytes and LLC cells (Fig. 6E and F). Most importantly, SIRT6 overexpression increased total ATP production in cardiomyocytes but significantly decreased total ATP production in LLC cells (Fig. 6E and F), which supported our hypothesis that SIRT6-mediated metabolic remodeling protected cardiomyocytes but not cancer cells against Dox-induced cytotoxicity. Furthermore, SIRT6 overexpression reversed the Dox-induced reduction in ATP production in cardiomyocytes while synergistically enhancing the Dox-induced reduction in ATP production in LLC cells (Fig. 6E and F), which may explain how SIRT6 can differentially regulate Dox-induced cytotoxicity in cardiomyocytes and cancer cells.

To elucidate how SIRT6 differentially regulates ATP production, the proportion of ATP produced by these two metabolic patterns among total ATP production was statistically analyzed. Dox treatment significantly increased the percentage of ATP produced by glycolysis and decreased the percentage of ATP produced by mitochondrial respiration in cardiomyocytes and LLC cells compared to untreated cells (Fig. 6G and H). Conversely, cells overexpressing SIRT6 exhibited a lower percentage of ATP produced by glycolysis and a higher percentage of

determining the fluorescence ratio of 586 nm/440 nm in (G) cells infected with lentivirus containing the SGK1 vector or control vector and (H) cells transfected with SGK1 siRNA or control siRNA ($n = 3$ different experiments). (I, J) ChIP analyses were used to detect SIRT6 binding and H3K9 acetylation at the *Sgk1* promoter in the cardiac tissue of SIRT6 KO mice and WT littermates, as well as LLC cells transfected with SIRT6 siRNA or control siRNA, which were performed with SIRT6, Ach3K9 antibodies and IgG control antibody. The results are shown relative to the background IgG antibody ($n = 3$ different experiments). The data are expressed as the mean \pm standard deviation. Two-tailed unpaired *t* tests were performed to determine significant differences in C–D and I–J. One-way ANOVA followed by Bonferroni multiple comparisons were performed to determine significant differences in E–H. * $P < 0.05$, ** $P < 0.01$, and *** $P < 0.001$. n.s., no significance.

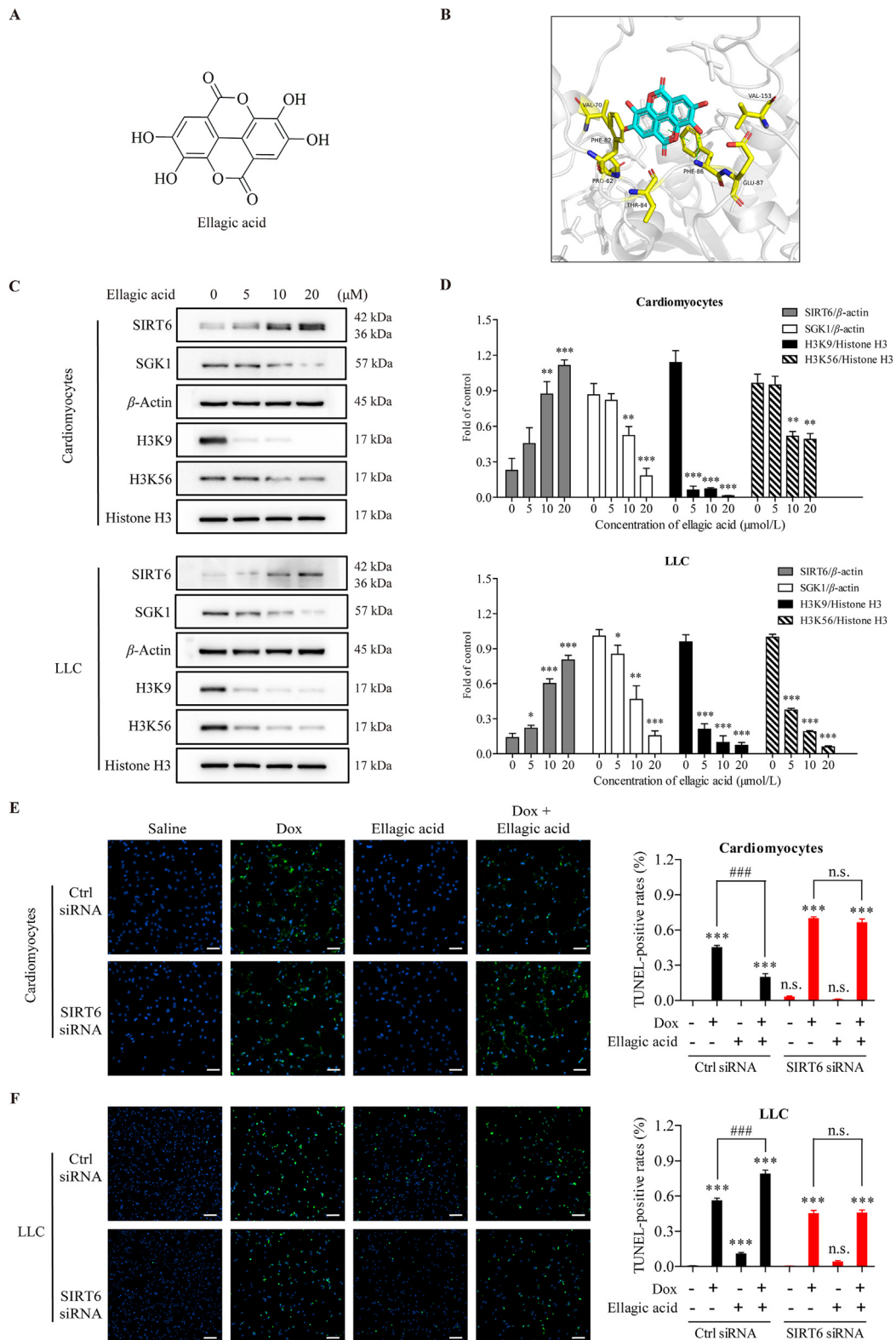


Figure 8 Ellagic acid-induced SIRT6 overexpression ameliorates Dox-induced cytotoxicity in cardiomyocytes but exacerbates Dox-induced cytotoxicity in cancer cells. (A) The 2D structure of ellagic acid. (B) The 3D binding model of ellagic acid and SIRT6. The ellagic acid is colored in cyan. The surrounding residues in the binding pocket are colored in yellow. The backbone of the receptor is depicted as gray cartoon. The hydrogen bond and Pi-Pi stacking interaction are depicted as green dashed lines. (C, D) After treatment with different concentrations of ellagic acid for 24 h, the expression of SIRT6, SGK1, H3K9 and H3K56 in primary cardiomyocytes isolated from WT mice and LLC cells was examined by Western blotting. β-Actin was used as a loading control. Semiquantitative analyses of bands were performed using ImageJ software ($n = 3$ different experiments). (E, F) Primary cardiomyocytes isolated from WT mice and LLC cells were transfected with SIRT6 siRNA or

ATP produced by mitochondrial respiration than control cells (Fig. 6G and H). The Dox-induced increase in glycolysis and decrease in mitochondrial respiration were effectively reversed by SIRT6 overexpression (Fig. 6G and H), which further confirmed that SIRT6 mediated a metabolic shift from glycolysis to mitochondrial respiration during Dox treatment.

Taken together, these results suggest that SIRT6 overexpression could coordinate a switch from glycolysis to mitochondrial respiration, which was more suitable for the metabolic pattern of cardiomyocytes, thus differentially regulating Dox-induced reduction in ATP production in cardiomyocytes and LLC cells. These results elucidate the mechanism by which SIRT6 overexpression protects cardiomyocytes but not cancer cells against Dox-induced cytotoxicity.

3.7. SIRT6 regulates mitochondrial biogenesis and mitophagy by deacetylating and inhibiting *Sgk1*

Our results showed that SIRT6 regulated metabolic remodeling from glycolysis to mitochondrial respiration. SIRT6 has been shown to inhibit glycolysis mainly by regulating the expression of glycolytic gene HIF1 α ^{29,40}. We re-confirmed this result by Western blotting, and the results showed that SIRT6 overexpression increased the protein level of HIF1 α , and SIRT6 knockout/knockdown decreased the protein level of HIF1 α (Supporting Information Fig. S3). However, the role of SIRT6 in modulating mitochondrial respiration by maintaining mitochondrial homeostasis is not yet clear. By monitoring markers of mitochondrial biogenesis and mitophagy in the myocardium and LLC cells, we found that SIRT6 overexpression increased the protein level of PGC1 α , a marker of mitochondrial biogenesis, and SIRT6 knockout/knockdown decreased the protein level of PGC1 α (Supporting Information Fig. S4A and S4B). Moreover, the protein level of TOMM20, a marker of the mitochondrial outer membrane, was increased by SIRT6 overexpression and decreased by SIRT6 knockout/knockdown (Fig. S4A and S4B). Furthermore, SIRT6 overexpression increased the protein levels of BNIP3, BNIP3L/Nix and Parkin, which are markers of mitophagy, and SIRT6 knockout/knockdown decreased the levels of these proteins (Fig. S4A and S4B). These results suggested that mitochondrial biogenesis and mitophagy could be activated by SIRT6 overexpression and inhibited by SIRT6 knockout/knockdown. In addition, SIRT6 overexpression led to an increase in the number of mitochondria, as assessed by increased level of MitoTracker staining and the ratio of mtDNA to nucleic DNA, and SIRT6 knockout/knockdown decreased the number of mitochondria in cardiomyocytes and LLC cells (Fig. S4C–S4F). Furthermore, SIRT6 overexpression led to an increase in the mitophagy levels of cardiomyocytes and LLC cells, as assessed by increased colocalization of mitochondria and lysosomes (Fig. S4G and S4H). Collectively, these results demonstrate that SIRT6 could modulate mitochondrial respiration by regulating mitochondrial biogenesis and mitophagy.

Since SIRT6 is localized to the cell nucleus but not to mitochondria²³, we hypothesized that SIRT6 could indirectly modulate mitochondrial biogenesis and mitophagy by transcriptionally regulating other genes. To examine the genes regulated by SIRT6, we performed RNA sequencing on primary cardiomyocytes isolated from SIRT6 TG mice and WT mice in the presence or absence of Dox. In the absence of Dox, 215 differentially expressed genes were found between WT and TG cardiomyocytes. KEGG analysis indicated that these genes were highly enriched in the PI3K/Akt signaling pathway (Fig. 7A), and the expression levels of the 14 enriched genes in the PI3K/Akt signaling pathway are shown in the clustering heatmap (Fig. 7B). In the presence of Dox, 159 differentially expressed genes were found between WT and TG cardiomyocytes, which were also highly enriched in the PI3K/Akt signaling pathway (Supporting Information Fig. S5A and S5B). Moreover, 79 genes were found in the overlap region between the two gene sets (Fig. S5C), and 16 genes were screened out of the 79 genes by increasing the screening standard (Fig. S5D). Among the genes that were screened out of the different analyses, we were most interested in a gene known as *Sgk1* (serum/glucocorticoid regulated kinase-1), which was found in all three clustering heatmaps (Figs. 7B, S5B and S5D, and Supporting Information Table S2). The results showed that the transcription of *Sgk1* was inhibited by SIRT6 (Fig. 7B). Moreover, the protein level of SGK1 was decreased by SIRT6 overexpression and increased by SIRT6 knockout/knockdown (Fig. 7C and D), which further confirmed the results of the gene expression analysis.

Since SGK1 has been reported to regulate mitochondrial homeostasis^{43–45}, we explored whether SIRT6 could regulate mitochondrial biogenesis and mitophagy by inhibiting SGK1 expression. In cardiomyocytes and LLC cells, SGK1 overexpression decreased the number of mitochondria, whereas SGK1 knockdown increased the number of mitochondria, as assessed by the ratios of mtDNA to nucleic DNA (Fig. 7E and F). Notably, the increase in mitochondrial number induced by SIRT6 overexpression was completely inhibited by SGK1 overexpression, and the decrease in mitochondrial number induced by SIRT6 knockout/knockdown was completely abrogated by SGK1 knockdown (Fig. 7E and F), suggesting that SIRT6 regulated mitochondrial biogenesis by modulating SGK1. Similar to these results, SGK1 overexpression slightly decreased mitophagy levels but significantly inhibited the effects of SIRT6 overexpression on mitophagy levels, as measured by a mitophagy reporter (Fig. 7G and H). Conversely, SGK1 knockdown increased mitophagy levels and abrogated the inhibitory effects of SIRT6 knockout/knockdown on mitophagy (Fig. 7G and H). Taken together, these results confirm that SIRT6-inhibited SGK1 expression was responsible for the effects on mitochondrial biogenesis and mitophagy. In addition, as an important product of mitochondrial damage, mitochondrial ROS (mitoROS) was also detected by a Mito-SOX mitochondrial superoxide indicator. SIRT6 overexpression significantly decreased Dox-induced mitoROS accumulation (Supporting Information Fig. S6). Notably, the

control siRNA. After pre-treated with ellagic acid (10 μ mol/L) for 24 h, Dox (0.5 μ mol/L) was added to culture medium for subsequent 24 h, and apoptosis was analyzed by TUNEL assays. Representative images are shown (scale bar = 100 μ m). The TUNEL-positive rates were quantified blindly in 5 images from different fields. The data are expressed as the mean \pm standard deviation. Two-tailed unpaired *t* tests were performed to determine significant differences in D. One-way ANOVA followed by Bonferroni multiple comparisons were performed to determine significant differences in E and F. **P* < 0.05, ***P* < 0.01, and ****P* < 0.001 compared to the control group. #*P* < 0.05, ##*P* < 0.01, and ###*P* < 0.001 compared to the Dox-treated group. n.s., no significance.

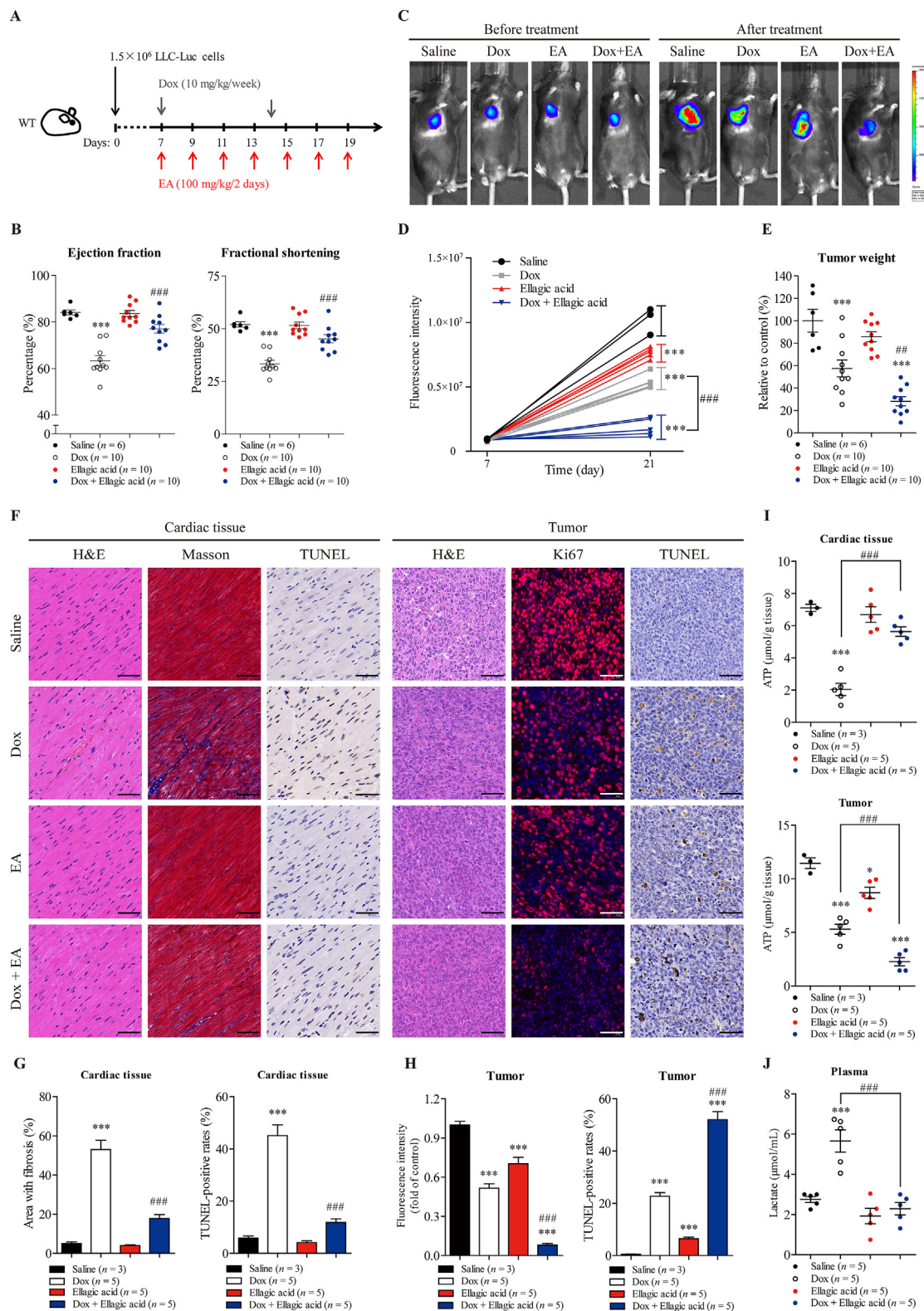


Figure 9 Ellagic acid alleviates Dox-induced cardiotoxicity and potentiates Dox-mediated tumor regression in mice. (A) The treatment protocol is shown. Wild-type C57BL/6 mice were inoculated subcutaneously with 1.5×10^6 LLC-Luc cells (LLC cells stably expressing the luciferase gene). After tumors became visible (approximately 7 days), the tumor-bearing mice were treated with Dox (10 mg/kg/week, i.v.) or/and ellagic acid (100 mg/kg/2 days, i.g.) for 2 weeks. (B) Cardiac function was measured using echocardiography as assessed by ejection fraction and fractional shortening in the mice. The diastolic left ventricular anterior wall thickness and diastolic left ventricular internal diameter are shown in [Supporting Information Fig. S8](#) ($n = 6$ or 10 animals per group). (C, D) Tumor volume was visualized using the IVIS Imaging System before and after treatment, and representative bioluminescence images and quantitative analyses of the tumor-bearing mice are shown ($n = 3$ or 5 animals

decrease in mitoROS induced by SIRT6 overexpression was significantly abrogated by SGK1 overexpression (Fig. S6), which further confirmed that SGK1 could function as a major downstream coordinator to mediate the effects of SIRT6 on mitochondrial homeostasis.

However, the mechanism by which SIRT6 regulates the transcription of *Sgk1* is still unknown. Because SIRT6 can function as a chromatin-associated deacetylase to regulate gene expression²⁴, we tested whether SIRT6 could directly regulate the transcription of *Sgk1* by modifying chromatin. According to the chromatin immunoprecipitation (ChIP) results, SIRT6 binding at the promoter of *Sgk1* was decreased in SIRT6-knockout myocardium compared with WT myocardium (Fig. 7I). The acetylation levels of H3K9 in the promoter of *Sgk1* were increased in SIRT6-knockout myocardium compared to WT myocardium (Fig. 7I). Similar results were observed in LLC cells, and there was decreased binding of SIRT6 and increased acetylation levels of H3K9 at the promoter of *Sgk1* in LLC cells with SIRT6 knock-down compared to control cells (Fig. 7J). These results indicate that SIRT6 directly inhibited the expression of *Sgk1* by deacetylating H3K9 at the *Sgk1* promoter.

3.8. Ellagic acid alleviates Dox-induced cardiotoxicity and potentiates Dox-mediated tumor regression

It has been confirmed that ellagic acid (EA) can function as a SIRT6 activator to increase SIRT6 expression in cancer cells⁴⁶. Thus, we investigated whether ellagic acid could alleviate cardiac dysfunction induced by Dox while simultaneously enhancing the antitumor efficacy of Dox by activating SIRT6.

To explore binding affinity of the ellagic acid with SIRT6, MOE-Dock simulation study was carried out. The 2D structure of ellagic acid is shown in Fig. 8A, the binding model of ellagic acid and SIRT6 is depicted in Fig. 8B, and the docking score is -5.0383 kcal/mol. Ellagic acid has formed a suitable steric complementarity with the binding site of SIRT6. Otherwise, hydrogen bond and Pi–Pi stacking interaction were formed among ellagic acid and SIRT6. The oxygen atom in the OH group of ellagic acid, regarded as hydrogen bond receptor, formed a hydrogen bond with the nitrogen atom in the backbone of Phe86 in SIRT6. And the benzene ring of Phe86 formed Pi–Pi stacking interaction with the oxygen heterocyclic of ellagic acid. VDW interactions were also formed among ellagic acid and SIRT6. These interactions mainly contributed to the binding energy between ellagic acid and SIRT6. To further validate the binding sites of the ellagic acid, we mutated the residues that involved in the binding of ellagic acid at the SIRT6 allosteric site, and the deacetylase activity of SIRT6 after treated with ellagic acid was evaluated by Fluor de Lys (FDL) assay⁴⁷. The mutation of Phe86 to alanine (F86A) decreased the half-maximal effective

concentration (EC₅₀) value (Supporting Information Fig. S7), which confirmed ellagic acid activates SIRT6 deacetylation by binding to the allosteric site.

To confirm whether ellagic acid-activated SIRT6 could differentially regulate Dox-induced apoptosis in cardiomyocytes and cancer cells, we isolated primary cardiomyocytes from WT mice, and treated cardiomyocytes and LLC cells with Dox in the presence or absence of ellagic acid. Treatment with ellagic acid increased the expression of SIRT6 and decreased the acetylation of lysines 9 and 56 of histone H3 (H3K9 and H3K56) in a dose-dependent manner (Fig. 8C and D), which further confirmed the activation of SIRT6 by ellagic acid. In addition, treatment with ellagic acid increased SGK1 expression in a dose-dependent manner (Fig. 8C and D). Moreover, ellagic acid treatment decreased Dox-induced cardiomyocyte apoptosis, as assessed by TUNEL staining (Fig. 8E). Notably, the prevention of Dox-mediated apoptosis by ellagic acid was completely abrogated in SIRT6-deficient cardiomyocytes (Fig. 8E). Conversely, ellagic acid treatment enhanced Dox-induced apoptosis in LLC cells (Fig. 8F). Similar to the results in cardiomyocytes, the enhancement of Dox-mediated apoptosis by ellagic acid was completely abrogated in SIRT6-deficient LLC cells (Fig. 8F). These results suggest that ellagic acid could limit Dox-induced apoptosis in cardiomyocytes and enhance Dox-induced apoptosis in cancer cells, and these effects were mainly dependent on ellagic acid-mediated SIRT6 activation.

To investigate whether ellagic acid could alleviate Dox-induced cardiac dysfunction and potentiate the antitumor efficacy of Dox *in vivo*, wild-type C57BL/6 mice bearing tumors derived from LLC cells were treated with ellagic acid and Dox individually or in combination. Cardiotoxicity and antitumor efficacy were examined in the same animals (Fig. 9A).

First, cardiotoxicity was assessed at the time of treatment termination. Dox treatment induced cardiac dysfunction, as assessed by decreases in EF, FS, LVAWd and LVIDd, compared to that in saline-treated mice (Fig. 9B and Supporting Information Fig. S8A and S8B). Treatment with ellagic acid did not independently alter cardiac function compared to saline treatment, but effectively ameliorated Dox-induced cardiac dysfunction (Figs. 9B and S8A and S8B). Moreover, co-treatment with ellagic acid significantly reversed the Dox-mediated increase in biochemical parameters associated with heart failure, including LDH, LDH1, CK and CK-MB (Fig. S8C). In addition, ellagic acid significantly decreased Dox-induced apoptosis and fibrosis in the myocardium, as measured by TUNEL and Masson trichrome staining, respectively (Fig. 9F and G). These results confirm that ellagic acid could significantly alleviate Dox-induced cardiotoxicity.

Second, the effects of ellagic acid on the antitumor efficacy of Dox were examined in same animal models. Luminescence analysis of tumors showed that treatment with ellagic acid or Dox

per group). (E) At treatment termination, tumors from each mouse were excised and weighed, and photographs of the tumors are shown in Fig. S8 ($n = 6$ or 10 animals per group). (F) Cell morphology, fibrosis and apoptosis in the cardiac tissue of the tumor-bearing mice were examined by H&E, Masson and TUNEL staining, respectively. Cell morphology, proliferation and apoptosis and in the tumors were measured by H&E, Ki67 immunofluorescence and TUNEL staining, respectively. Representative images are shown (scale bar = $50 \mu\text{m}$). (G, H) Quantitative analyses of the fibrotic area (blue-stained), TUNEL-positive cells (brown-stained) and fluorescence of Ki67 (red-stained) in F were performed by ImageJ software ($n = 3$ or 5 animals per group). (I) ATP concentrations in cardiac tissue and tumors were measured ($n = 3$ or 5 animals per group). (J) The lactate concentration in the plasma of tumor-bearing mice was measured ($n = 3$ or 5 animals per group). The data are expressed as the mean \pm standard error of mean. One-way ANOVA followed by Bonferroni multiple comparisons were performed to determine significant differences. * $P < 0.05$, ** $P < 0.01$, and *** $P < 0.001$ compared to saline-treated mice. # $P < 0.05$, ## $P < 0.01$, and ### $P < 0.001$ compared to Dox-treated mice.

alone suppressed tumor growth compared to saline treatment (Fig. 9C and D). Notably, ellagic acid significantly potentiated Dox-mediated tumor regression (Fig. 9C and D). Moreover, ellagic acid did not independently decrease tumor weight compared to saline treatment but effectively enhanced the anti-tumor effect of Dox (Fig. 9E and Fig. S8D). And there were significant differences in tumor weight between the combined treatment group and the two single-drug treatment groups (Fig. 9E and Fig. S8D), suggesting that the combination of ellagic acid and Dox exhibited greater antitumor efficacy than either agent alone. In addition, ellagic acid significantly potentiated Dox-mediated pro-apoptotic and anti-proliferative activity in the tumor, as measured by TUNEL and Ki67 immunofluorescence staining, respectively (Fig. 9F and H). These results confirm that ellagic acid could significantly potentiate the antitumor efficacy of Dox.

Third, since SIRT6 differentially regulates Dox-mediated energy deficiency in cardiomyocytes and cancer cells *in vitro*, the concentration of ATP in both the myocardium and the tumor was examined. Compared to saline treatment, Dox treatment alone significantly decreased ATP concentrations in both the myocardium and the tumor, which may explain the cardiotoxicity and antitumor effect of Dox (Fig. 9I). Notably, treatment with ellagic acid did not independently alter ATP concentration in the myocardium compared to saline treatment, but effectively ameliorated the Dox-induced loss of energy production in the myocardium (Fig. 9I). Conversely, treatment with ellagic acid decreased ATP concentrations in tumors compared to those in the saline-treated group. Combination treatment with ellagic acid and Dox had a synergetic effect and decreased ATP concentrations in the tumor (Fig. 9I). These results indicate that ellagic acid could limit Dox-induced energy deficiency in the myocardium and enhance Dox-mediated energy deficiency in the tumor, which was consistent with our *in vitro* data. In addition, the combination treatment diminished Dox-induced lactate accumulation in plasma (Fig. 9J), suggesting that ellagic acid could suppress the Dox-induced increase in glycolysis *in vivo*. Furthermore, treatment with ellagic acid increased the expression of SIRT6 in both the myocardium and tumors (Fig. S8F and S8G), indicating that ellagic acid could be used as an effective SIRT6 activator *in vivo*.

Collectively, these results suggested that ellagic acid alleviated Dox-induced cardiotoxicity while simultaneously enhancing Dox-mediated tumor regression, and these effects may be related to its effects on metabolic regulation and SIRT6 activation.

4. Discussion

Despite the noteworthy cardiotoxicity, Dox and related anthracyclines have been widely used in the clinic to treat various cancers. A previous study reported that the cardiotoxicity of Dox was cumulative-dose dependent, and the incidence of left ventricular systolic dysfunction sharply increased when the cumulative dose of Dox reached 400 mg/m²⁶. It has been reported that up to 7% of cancer patients develop left ventricular systolic dysfunction after receiving a cumulative dose of 150 mg/m² Dox⁶. A cohort study also reported that the incidence of left ventricular systolic dysfunction was 9%, and most cases of cardiomyopathy occurred within the first year of treatment⁴⁸. Considering the large number of cancer patients undergoing Dox treatment, even a low incidence of cardiomyopathy development represents a significant number of individuals³¹, which makes it imperative to explore the mechanism underlying the cardiotoxicity of Dox.

In recent years, several theories have been proposed to explain the mechanism of cardiotoxicity, including the accumulation of reactive oxygen species (ROS) and defects in iron handling^{49,50}. It has been reported that ROS accumulation induced by Dox could suppress mitochondrial function by impairing DNA integrity and decreasing mitochondrial membrane potential. Moreover, Dox could also directly hinder mitochondrial function by inhibiting electron transport chain protein expression and promoting mPTP opening⁵¹. Since mitochondrial respiration provides the majority of the energy required for cardiomyocyte pulsation and the pumping activity of the heart⁴², we could speculate that Dox-induced impairments in mitochondrial function lead to cardiac energy starvation. In addition, mitochondria are also considered as the regulators of apoptosis and necrosis, so defective mitochondria would lead to cardiomyocyte death. Hence, the evidence above suggested that mitochondria may be a convergence point for Dox-induced cardiotoxicity^{14,39}.

However, the mechanisms underlying Dox-induced cardiotoxicity are incompletely understood. In this study, we found that Dox-mediated mtDNA damage severely impaired mitochondrial respiration, which subsequently led to increased glycolysis to compensate for the loss of energy production. Moreover, oxrased-induced hypoxia saturated the cytotoxic effects of Dox in cardiomyocytes, which confirmed the above hypothesis. Hence, our results indicate that defective mitochondrial function and increased glycolysis are responsible for Dox-induced cardiotoxicity, as abnormal metabolic remodeling is an integral process associated with heart failure^{52,53}. A recent study confirmed that Dox-induced loss of mtDNA contributes to cardiomyopathy pathogenesis³¹, which supported our results. These findings suggested that antagonizing the abnormal metabolic pattern induced by Dox may prove beneficial in ameliorating Dox-induced cardiotoxicity.

A previous study confirmed that SIRT6-deficient embryonic stem cells and cancer cells exhibit increased glycolysis and diminished mitochondrial respiration, which were similar to the Dox-induced metabolic phenotype observed in this study^{29,40}. In this work, we found that SIRT6 overexpression induced metabolic remodeling from glycolysis to mitochondrial respiration in both cardiomyocytes and cancer cells, which suppressed Dox-activated glycolysis and reversed the Dox-mediated reduction in mitochondrial respiration. These results confirmed that SIRT6 overexpression could reverse the abnormal metabolic pattern induced by Dox.

Generally, most cancer cells exhibit a metabolic signature that consumes large amounts of glucose and primarily use glycolysis to produce ATP, even in the presence of adequate oxygen, which provides sufficient energy for their rapid growth and proliferation⁴¹. Conversely, fatty acids are the primary energy source of the heart, and glucose provides 20%–30% of the total cardiac energy requirement⁴². Notably, mitochondrial respiration contributes 95% of the ATP requirements of the myocardium, and glycolysis provides the remaining 5%. Under pathological conditions, increased glycolysis and impaired clearance of pyruvate lead to lactate accumulation in the myocardium, which is a feature of heart failure^{52,53}. Therefore, we hypothesized that SIRT6-mediated metabolic remodeling from glycolysis to mitochondrial respiration during Dox treatment was more suitable for the survival of cardiomyocytes than cancer cells. As expected, our results showed that SIRT6 overexpression increased total ATP production in cardiomyocytes by increasing mitochondrial respiration, which reversed the Dox-induced reduction in ATP production of

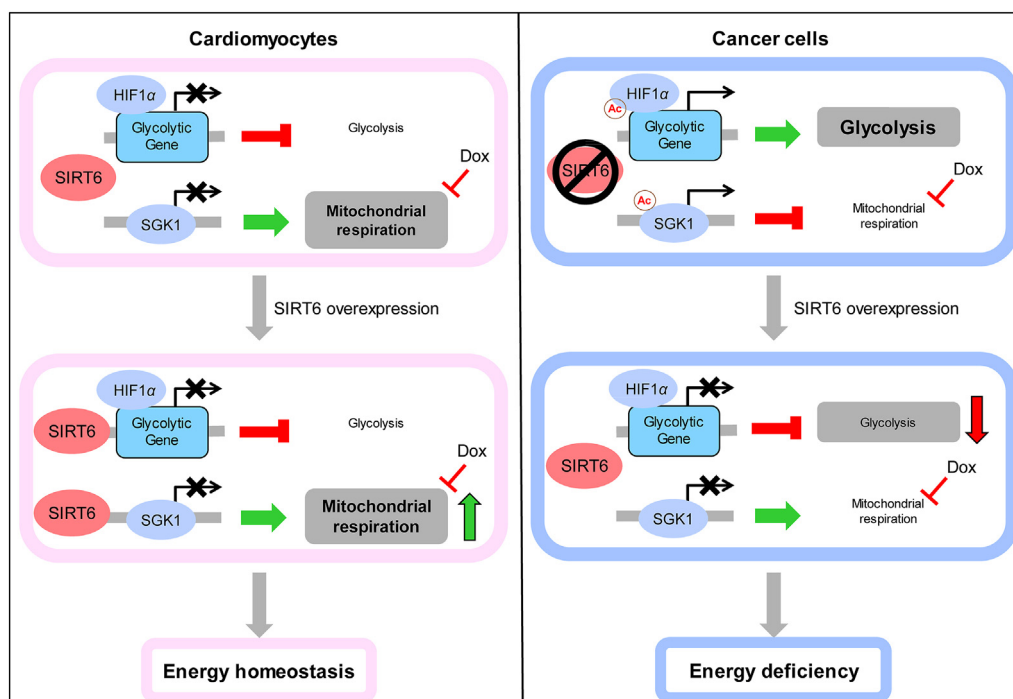


Figure 10 Schematic framework of the SIRT6-mediated differential responses to Dox between cardiomyocytes and cancer cells. Dox-impaired mitochondrial DNA led to metabolic remodeling of decreased mitochondrial respiration and increased glycolysis, thus inhibiting cellular ATP production, which were responsible for Dox-induced cytotoxicity. SIRT6 has been reported to function as a histone H3K9 deacetylase and inhibits the transcription of multiple glycolytic genes. Meanwhile, SIRT6 regulated mitochondrial biogenesis and mitophagy to maintain mitochondrial homeostasis by deacetylating and inhibiting SGK1, thus improving mitochondrial respiration when mitochondrial function is impaired by Dox. Thus, the differences in metabolic patterns between cardiomyocytes and cancer cells are responsible for the differential regulation of SIRT6 on energy production. In cardiomyocytes that depend on mitochondrial respiration for energy production, SIRT6 overexpression reversed the Dox-induced reduction in ATP production and improved cellular energy supply by increasing mitochondrial respiration. In cancer cells that depend on glycolysis for energy production, SIRT6 overexpression enhanced the Dox-induced reduction in ATP production and aggravated cellular energy deficiency by inhibiting glycolysis. Therefore, SIRT6 overexpression effectively reversed Dox-induced metabolic remodeling by increasing mitochondrial respiration and inhibiting glycolysis, which differentially regulated ATP production in cardiomyocytes and cancer cells.

cardiomyocytes. However, in LLC cells that depend on glycolysis for energy production, SIRT6 overexpression significantly decreased total ATP production by inhibiting glycolysis, which synergistically enhanced the Dox-induced reduction in ATP production. These results highlighted that SIRT6-mediated metabolic remodeling protects cardiomyocytes but not cancer cells against Dox-induced energy deficiency.

Mechanistically, SIRT6 has been reported to function as a histone H3K9 deacetylase and regulates the transcription of glycolytic genes^{29,40}. However, the molecular mechanism underlying SIRT6-increased mitochondrial respiration is not yet clear. In this study, we found that SIRT6 could enhance mitochondrial biogenesis and mitophagy by inhibiting SGK1 expression in both cardiomyocytes and LLC cells, which was responsible for the increase in mitochondrial respiration. Moreover, we also confirmed that SIRT6 directly inhibited the expression of *Sgk1* by deacetylating H3K9 at the *Sgk1* promoter. As a member of the AGC family of serine/threonine kinases, SGK1 has been reported to regulate mitophagy and mitochondrial homeostasis through multiple pathways^{43–45}. A previous study suggested that mTORC2/SGK1 knockdown increased the mitochondrial respiration rate in mammalian cells⁵⁴, and a recent study showed an increase in oxygen consumption in *Sgk-1* mutant worms⁴⁵, which supported our results that SIRT6-enhanced mitochondrial

respiration depended on the effects on SGK1-mediated mitochondrial biogenesis and the clearance of abnormal mitochondria. In addition, cardiac-specific inhibition of SGK1 was reported to protect mice against cardiac fibrosis and heart failure, which further confirmed that SIRT6-mediated SGK1 inhibition could be beneficial in the treatment of cardiac disease⁵⁵. Overall, SIRT6 could act as a histone H3K9 deacetylase to inhibit glycolysis and enhance mitochondrial respiration, thus leading to metabolic remodeling, which is suitable for the metabolic pattern of cardiomyocytes (Fig. 10).

By abrogating the abnormal metabolic pattern induced by Dox, SIRT6 overexpression demonstrated promising effects against Dox-induced cardiotoxicity, and significantly potentiated the antitumor efficacy of Dox. Our *in vitro* results show that SIRT6 overexpression decreased Dox-induced cytotoxicity in cardiomyocytes and potentiated the anticancer efficacy of Dox against cancer cells. Moreover, SIRT6 overexpression effectively ameliorated Dox-induced cardiac dysfunction, fibrosis and apoptosis in mice. In an acute cardiotoxicity model treated with high-dose Dox, overall survival of mice was prolonged by SIRT6 overexpression. Moreover, a recent study had confirmed that miR-330-5p could ameliorate doxorubicin-induced cardiotoxicity through up-regulating SIRT6, which also suggested SIRT6 could be a potential target for the cardiotoxicity⁵⁶. In addition, our

in vivo results also showed that Dox exhibited greater antitumor efficacy in LLC tumors with SIRT6 overexpression than in control LLC tumors, suggesting that SIRT6 overexpression could significantly potentiate the antitumor efficacy of Dox. In addition, we observed that reduced SIRT6 expression was relevant to anthracyclines-induced cardiotoxicity in humans. These results confirmed that SIRT6 overexpression could be an effective adjunctive strategy during treatment of Dox.

In addition, other mechanisms may be also related to the protective effects of SIRT6 on Dox-induced cardiotoxicity, besides the energy metabolism. For example, a recent study found that SIRT6 deficiency enhances the expression of fatty acid transporters, leading to enhanced fatty acid uptake and lipid accumulation⁵⁷. Generally, excessive accumulation of lipids compromises cardiac function⁵⁸. These works suggest that targeting SIRT6 may be beneficial in reducing cardiac lipotoxicity, and implied that the decreased accumulation of lipid may mediate the protective effects of SIRT6 on Dox-induced cardiotoxicity. However, the hypothesis still needs further study to confirm.

To date, some novel compounds that activate SIRT6 have been designed in preclinical works^{47,59,60}, but there are still no SIRT6 activator has been used in clinical trials for the treatment of human diseases. Given the challenges of pharmacologically activating SIRT6, ellagic acid, a natural compound that is present in many fruits, such as raspberry, cloudberry, blackberry and pomegranate, was used in this study⁶¹. Notably, a previous work confirmed that ellagic acid increased the deacetylase activity of SIRT6 by up to 50-fold in colorectal cancer cells⁴⁶. In this study, ellagic acid limited Dox-induced apoptosis in cardiomyocytes and enhanced Dox-induced apoptosis in cancer cells, and these effects were mainly dependent on ellagic acid-mediated SIRT6 activation. Moreover, ellagic acid could alleviate Dox-induced heart failure and enhance Dox-mediated tumor regression in tumor-bearing mice, which is similar to the therapeutic effects of CR^{16–19}. A previous study also confirmed the cardio-protective effects of ellagic acid⁶², which confirmed our results. These results suggested that SIRT6 activation by ellagic acid could be a novel preventive and therapeutic agent for chemotherapy-induced cardiotoxicity.

Given the vital role of mitochondrial homeostasis in cardiac function, our findings suggested that interventions designed to activate SIRT6 could be beneficial for other types of heart failure beyond anthracyclines-induced cardiotoxicity. A previous study found that SIRT6 knockout worsened cardiac damage, which further confirmed the protective effects of SIRT6 on cardiovascular disease⁶³. Similarly, our findings also indicated that targeting SIRT6 could also be effective in enhancing the therapeutic response to chemotherapy in other cancer types that depend on glycolysis.

5. Conclusions

Collectively, our findings highlight the crucial role of SIRT6 in mitochondrial homeostasis and suggest targeting SIRT6 activation as a feasible and promising strategy for the prevention or treatment of anthracycline-induced cardiotoxicity. Our work also provides a preclinical rationale for using ellagic acid as a potential adjunctive therapy in cancer patients undergoing chemotherapy.

Acknowledgments

This work was supported by the National Natural Science Foundation of China (81871095 and 82170873), the National Key R&D Program of China (2018YFC2000304), the Tsinghua

Precision Medicine Foundation (10001020132, China), and the Tsinghua University Spring Breeze Fund (20211080005, China).

Author contributions

Zhao Wang supervised the study. Zhao Wang, Ying Qiu and Mingkui Zhang funded the study. Kezheng Peng and Zhao Wang designed the experiments. Kezheng Peng, Yuqi Gao and Chenye Zeng performed the experiments. Kezheng Peng, Yuqi Gao, Liyuan Li and Yuemiao Yin analyzed the data. Kezheng Peng and Kang Xu generated the animal models. Binliang Liu and Fei Ma collected the clinic samples. Kezheng Peng and Zhao Wang wrote the manuscript. All the authors read and discussed the manuscript.

Conflicts of interest

The authors declare no conflicts of interest.

Appendix A. Supporting information

Supporting data to this article can be found online at <https://doi.org/10.1016/j.japsb.2023.03.019>.

References

1. Rayson D, Richel D, Chia S, Jackisch C, van der Vegt S, Suter T. Anthracycline-trastuzumab regimens for HER2/neu-overexpressing breast cancer: current experience and future strategies. *Ann Oncol* 2008;**19**:1530–9.
2. Zamorano JL, Lancellotti P, Rodríguez Muñoz D, Aboyans V, Asteggiano R, Galderisi M, et al. 2016 ESC position paper on cancer treatments and cardiovascular toxicity developed under the auspices of the ESC committee for practice guidelines: the task force for cancer treatments and cardiovascular toxicity of the European Society of Cardiology (ESC). *Eur J Heart Fail* 2017;**19**:9–42.
3. Carvalho FS, Burgeiro A, Garcia R, Moreno AJ, Carvalho RA, Oliveira PJ. Doxorubicin-induced cardiotoxicity: from bioenergetic failure and cell death to cardiomyopathy. *Med Res Rev* 2014;**34**:106–35.
4. Hayek ER, Speakman E, Rehmus E. Acute doxorubicin cardiotoxicity. *N Engl J Med* 2005;**352**:2456–7.
5. Steinherz LJ, Steinherz PG, Tan CT, Heller G, Murphy ML. Cardiac toxicity 4 to 20 years after completing anthracycline therapy. *JAMA* 1991;**266**:1672–7.
6. Swain SM, Whaley FS, Ewer MS. Congestive heart failure in patients treated with doxorubicin: a retrospective analysis of three trials. *Cancer* 2003;**97**:2869–79.
7. Cardinale D, Caruso V, Cipolla CM. The breast cancer patient in the cardiology unit. *J Thorac Dis* 2018;**10**:S4306–22.
8. Moslehi J, Amgalan D, Kitsis RN. Grounding cardio-oncology in basic and clinical science. *Circulation* 2017;**136**:3–5.
9. Khoo KH, Verma CS, Lane DP. Drugging the p53 pathway: understanding the route to clinical efficacy. *Nat Rev Drug Discov* 2014;**13**:217–36.
10. Shizukuda Y, Matoba S, Mian OY, Nguyen T, Hwang PM. Targeted disruption of p53 attenuates doxorubicin-induced cardiac toxicity in mice. *Mol Cell Biochem* 2005;**273**:25–32.
11. Sano M, Minamino T, Toko H, Miyauchi H, Orimo M, Qin Y, et al. p53-induced inhibition of Hif-1 causes cardiac dysfunction during pressure overload. *Nature* 2007;**446**:444–8.
12. Saleme B, Gurtu V, Zhang Y, Kinnaird A, Boukouris AE, Gopal K, et al. Tissue-specific regulation of p53 by PKM2 is redox dependent and provides a therapeutic target for anthracycline-induced cardiotoxicity. *Sci Transl Med* 2019;**11**:eaau8866.

13. Zhu W, Zhang W, Shou W, Field LJ. P53 inhibition exacerbates late-stage anthracycline cardiotoxicity. *Cardiovasc Res* 2014;**103**:81–9.
14. Dhingra R, Margulets V, Chowdhury SR, Thliveris J, Jassal D, Fernyhough P, et al. Bnip3 mediates doxorubicin-induced cardiac myocyte necrosis and mortality through changes in mitochondrial signaling. *Proc Natl Acad Sci U S A* 2014;**111**:E5537–44.
15. Longo VD, Mattson MP. Fasting: molecular mechanisms and clinical applications. *Cell Metab* 2014;**19**:181–92.
16. Lee C, Raffaghello L, Brandhorst S, Safdie FM, Bianchi G, Martin-Montalvo A, et al. Fasting cycles retard growth of tumors and sensitize a range of cancer cell types to chemotherapy. *Sci Transl Med* 2012;**4**:124ra27.
17. Lee C, Safdie FM, Raffaghello L, Wei M, Madia F, Parrella E, et al. Reduced levels of IGF-I mediate differential protection of normal and cancer cells in response to fasting and improve chemotherapeutic index. *Cancer Res* 2010;**70**:1564–72.
18. Raffaghello L, Lee C, Safdie FM, Wei M, Madia F, Bianchi G, et al. Starvation-dependent differential stress resistance protects normal but not cancer cells against high-dose chemotherapy. *Proc Natl Acad Sci U S A* 2008;**105**:8215–20.
19. de Groot S, Lugtenberg RT, Cohen D, Welters MJ, Ehsan I, Vreeswijk MP, et al. Fasting mimicking diet as an adjunct to neo-adjuvant chemotherapy for breast cancer in the multicentre randomized phase 2 DIRECT trial. *Nat Commun* 2020;**11**:3083.
20. Clifton KK, Ma CX, Fontana L, Peterson LL. Intermittent fasting in the prevention and treatment of cancer. *CA Cancer J Clin* 2021;**71**:527–46.
21. Rhoads TW, Burhans MS, Chen VB, Hutchins PD, Rush MJ, Clark JP, et al. Caloric restriction engages hepatic RNA processing mechanisms in rhesus monkeys. *Cell Metab* 2018;**27**:677–688.e5.
22. Roichman A, Elhanati S, Aon MA, Abramovich I, Di Francesco A, Shahar Y, et al. Restoration of energy homeostasis by SIRT6 extends healthy lifespan. *Nat Commun* 2021;**12**:3208.
23. Kugel S, Mostoslavsky R. Chromatin and beyond: the multitasking roles for SIRT6. *Trends Biochem Sci* 2014;**39**:72–81.
24. Kawahara TL, Michishita E, Adler AS, Damian M, Berber E, Lin M, et al. SIRT6 links histone H3 lysine 9 deacetylation to NF- κ B-dependent gene expression and organismal life span. *Cell* 2009;**136**:62–74.
25. Michishita E, McCord RA, Boxer LD, Barber MF, Hong T, Gozani O, et al. Cell cycle-dependent deacetylation of telomeric histone H3 lysine K56 by human SIRT6. *Cell Cycle* 2009;**8**:2664–6.
26. Tasselli L, Xi Y, Zheng W, Tennen RI, Odrowaz Z, Simeoni F, et al. SIRT6 deacetylates H3K18ac at pericentric chromatin to prevent mitotic errors and cellular senescence. *Nat Struct Mol Biol* 2016;**23**:434–40.
27. Zhou Y, Fan X, Jiao T, Li W, Chen P, Jiang Y, et al. SIRT6 as a key event linking P53 and NRF2 counteracts APAP-induced hepatotoxicity through inhibiting oxidative stress and promoting hepatocyte proliferation. *Acta Pharm Sin B* 2021;**11**:89–99.
28. Li Z, Xu K, Zhang N, Amador G, Wang Y, Zhao S, et al. Overexpressed SIRT6 attenuates cisplatin-induced acute kidney injury by inhibiting ERK1/2 signaling. *Kidney Int* 2018;**93**:881–92.
29. Sebastian C, Zwaans BM, Silberman DM, Gymrek M, Goren A, Zhong L, et al. The histone deacetylase SIRT6 is a tumor suppressor that controls cancer metabolism. *Cell* 2012;**151**:1185–99.
30. Kugel S, Sebastian C, Fitamant J, Ross KN, Saha SK, Jain E, et al. SIRT6 suppresses pancreatic cancer through control of Lin28b. *Cell* 2016;**165**:1401–15.
31. Li J, Wang PY, Long NA, Zhuang J, Springer DA, Zou J, et al. p53 prevents doxorubicin cardiotoxicity independently of its prototypical tumor suppressor activities. *Proc Natl Acad Sci U S A* 2019;**116**:19626–34.
32. Ehler E, Moore-Morris T, Lange S. Isolation and culture of neonatal mouse cardiomyocytes. *J Vis Exp* 2013;**79**:50154.
33. Gao Y, Hua R, Peng K, Yin Y, Zeng C, Guo Y, et al. High-starchy carbohydrate diet aggravates NAFLD by increasing fatty acids influx mediated by NOX2. *Food Sci Hum Wellness* 2023;**12**:1081–101.
34. Li L, Chen B, Zhu R, Li R, Tian Y, Liu C, et al. Fructus Ligustri Lucidi preserves bone quality through the regulation of gut microbiota diversity, oxidative stress, TMAO and Sirt6 levels in aging mice. *Aging* 2019;**11**:9348–68.
35. Bian C, Gao J, Wang Y, Li J, Luan Z, Lu H, et al. Association of SIRT6 circulating levels with urinary and glycometabolic markers in pre-diabetes and diabetes. *Acta Diabetol* 2021;**58**:1551–62.
36. Zhao Y, Bai X, Jia X, Lu Y, Cheng W, Shu M, et al. Age-related changes of human serum Sirtuin6 in adults. *BMC Geriatr* 2021;**21**:452.
37. Yan Z, Wang X, Liu YS, Xing XW, Zhang XG, Lu QH. Decreased serum SIRT6 as a novel predictor of coronary artery disease. *Eur Rev Med Pharmacol Sci* 2021;**25**:6660–9.
38. Zhang J, Li Y, Liu Q, Huang Y, Li R, Wu T, et al. Sirt6 alleviated liver fibrosis by deacetylating conserved lysine 54 on smad2 in hepatic stellate cells. *Hepatology* 2021;**73**:1140–57.
39. Wallace KB, Sardao VA, Oliveira PJ. Mitochondrial determinants of doxorubicin-induced cardiomyopathy. *Circ Res* 2020;**126**:926–41.
40. Zhong L, D'Urso A, Toiber D, Sebastian C, Henry RE, Vadysirisack DD, et al. The histone deacetylase Sirt6 regulates glucose homeostasis via Hif1 α . *Cell* 2010;**140**:280–93.
41. Vander Heiden MG, Cantley LC, Thompson CB. Understanding the Warburg effect: the metabolic requirements of cell proliferation. *Science* 2009;**324**:1029–33.
42. Lopaschuk GD, Karwi QG, Tian R, Wende AR, Abel ED. Cardiac energy metabolism in heart failure. *Circ Res* 2021;**128**:1487–513.
43. Zhou B, Kreuzer J, Kumsta C, Wu L, Kamer KJ, Cedillo L, et al. Mitochondrial permeability uncouples elevated autophagy and lifespan extension. *Cell* 2019;**177**:299–314.e16.
44. Aspernik H, Heimbucher T, Qi W, Gangurde D, Curic S, Yan Y, et al. Mitochondrial perturbations couple mTORC2 to autophagy in *C. elegans*. *Cell Rep* 2019;**29**:1399–13409.e5.
45. de la Cruz-Ruiz P, Hernando-Rodríguez B, Pérez-Jiménez MM, Rodríguez-Palero MJ, Martínez-Bueno MD, Pla A, et al. Prohibitin depletion extends lifespan of a TORC2/SGK-1 mutant through autophagy and the mitochondrial UPR. *Aging Cell* 2021;**20**:e13359.
46. Rahnasto-Rilla M, Järvenpää J, Huovinen M, Schroderus AM, Ihtola EL, Küblbeck J, et al. Effects of galloflavin and ellagic acid on sirtuin 6 and its anti-tumorigenic activities. *Biomed Pharmacother* 2020;**131**:110701.
47. Huang Z, Zhao J, Deng W, Chen Y, Shang J, Song K, et al. Identification of a cellularly active SIRT6 allosteric activator. *Nat Chem Biol* 2018;**14**:1118–26.
48. Cardinale D, Colombo A, Bacchiani G, Tedeschi I, Meroni CA, Veglia F, et al. Early detection of anthracycline cardiotoxicity and improvement with heart failure therapy. *Circulation* 2015;**131**:1981–8.
49. Ichikawa Y, Ghanefar M, Bayeva M, Wu R, Khechaduri A, Naga Prasad SV, et al. Cardiotoxicity of doxorubicin is mediated through mitochondrial iron accumulation. *J Clin Investig* 2014;**124**:617–30.
50. Simunek T, Sterba M, Popelova O, Adamcova M, Hrdina R, Gersl V. Anthracycline-induced cardiotoxicity: overview of studies examining the roles of oxidative stress and free cellular iron. *Pharmacol Rep* 2009;**61**:154–71.
51. Kuznetsov AV, Margreiter R, Amberger A, Saks V, Grimm M. Changes in mitochondrial redox state, membrane potential and calcium precede mitochondrial dysfunction in doxorubicin-induced cell death. *Biochim Biophys Acta* 2011;**1813**:1144–52.
52. Zhou B, Tian R. Mitochondrial dysfunction in pathophysiology of heart failure. *J Clin Investig* 2018;**128**:3716–26.
53. Bertero E, Maack C. Metabolic remodelling in heart failure. *Nat Rev Cardiol* 2018;**15**:457–70.
54. Schieke SM, Phillips D, McCoy JP Jr, Aponte AM, Shen RF, Balaban RS, et al. The mammalian target of rapamycin (mTOR) pathway regulates mitochondrial oxygen consumption and oxidative capacity. *J Biol Chem* 2006;**281**:27643–52.
55. Das S, Aiba T, Rosenberg M, Hessler K, Xiao C, Quintero PA, et al. Pathological role of serum- and glucocorticoid-regulated kinase 1 in adverse ventricular remodeling. *Circulation* 2012;**126**:2208–19.

56. Han D, Wang Y, Wang Y, Dai X, Zhou T, Chen J, et al. The tumor-suppressive human circular RNA circITCH sponges miR-330-5p to ameliorate doxorubicin-induced cardiotoxicity through upregulating SIRT6, Survivin, and SERCA2a. *Circ Res* 2020;**127**: e108–25.
57. Khan D, Ara T, Ravi V, Rajagopal R, Tandon H, Parvathy J, et al. SIRT6 transcriptionally regulates fatty acid transport by suppressing PPAR γ . *Cell Rep* 2021;**35**:109190.
58. Goldberg IJ, Trent CM, Schulze PC. Lipid metabolism and toxicity in the heart. *Cell Metab* 2012;**15**:805–12.
59. Lu S, Chen Y, Wei J, Zhao M, Ni D, He X, et al. Mechanism of allosteric activation of SIRT6 revealed by the action of rationally designed activators. *Acta Pharm Sin B* 2021;**11**:1355–61.
60. He T, Shang J, Gao C, Guan X, Chen Y, Zhu L, et al. A novel SIRT6 activator ameliorates neuroinflammation and ischemic brain injury via EZH2/FOXC1 axis. *Acta Pharm Sin B* 2021;**11**:708–26.
61. Alfei S, Turrini F, Catena S, Zunin P, Grilli M, Pittaluga AM, et al. Ellagic acid a multi-target bioactive compound for drug discovery in CNS? A narrative review. *Eur J Med Chem* 2019;**183**:111724.
62. Lin MC, Yin MC. Preventive effects of ellagic acid against doxorubicin-induced cardio-toxicity in mice. *Cardiovasc Toxicol* 2013;**13**:185–93.
63. Wu S, Lan J, Li L, Wang X, Tong M, Fu L, et al. Sirt6 protects cardiomyocytes against doxorubicin-induced cardiotoxicity by inhibiting P53/Fas-dependent cell death and augmenting endogenous antioxidant defense mechanisms. *Cell Biol Toxicol* 2023;**39**:237–58.